Single-molecule Ligand Response of Guanidine-IV riboswitch

Lingzhi Gao[1], Dian Chen[1] and Yu Liu[1,2]*

[1]State Key Laboratory of Microbial Metabolism, School of Life Sciences and Biotechnology, Shanghai Jiao Tong University, Shanghai 200240, China. [2]Shanghai Artificial Intelligence Laboratory, Shanghai 200232, China.

*Corresponding author: liuyu_sjtu@sjtu.edu.cn.

ABSTRACT

Riboswitches are non-coding RNA elements that can specifically sense ligands and regulate gene expression. A recent report introduced a type of riboswitch known as the guanidine-IV riboswitch, which responds to guanidine levels and controls the transcription of downstream genes. However, there is currently a lack of clarity regarding the mechanism by which the riboswitch senses guanidine and undergoes conformational changes. This lack of understanding has impeded the application of this riboswitch. Therefore, our study aimed to address this gap by investigating the conformational changes that occur in a guanidine-IV riboswitch RNA. We examined the aptamer, terminator, and full-length riboswitch using single-molecule fluorescence resonance energy transfer (smFRET). Our findings indicated that the aptamer portion was more sensitive to guanidine compared to the terminator and full-length riboswitch. Additionally, we mimicked the structural changes in the guanidine-IV riboswitch that occur during transcription at a single-nucleotide and single-molecule level using Position-specific Labelling of RNA (PLOR) and smFRET. The results showed that guanidine caused a less pronounced change in the riboswitch RNA after transcribing 88 nucleotides. Based on our findings, we have proposed a folding model for the guanidine-IV riboswitch in the absence and presence of guanidine.

Impact statement

The guanidine-IV riboswitch's aptamer domain exhibits a greater sensitivity towards guanidine in comparison to both the terminator and full-length riboswitch. This results in the riboswitch showcasing a narrow transcriptional window that is responsive to ligand binding. And a comprehensive structure-function model for the guanidine-IV riboswitch under both guanidine-free and guanidine-present conditions.

INTRODUCTION

Riboswitches, located at the 5′-untranslated region of mRNA, are capable of regulating gene expression through structural changes after binding to their specific ligands (Jones & Ferre-D'Amare, 2017; Mandal & Breaker, 2004; Serganov & Nudler, 2013; Sherlock & Breaker, 2020). A typical riboswitch consists of an aptamer domain and an expression platform. The aptamer domain binds to a specific ligand, leading to structural changes and regulation of gene expression (Garst et al., 2011; Kavita & Breaker, 2023; Winkler & Breaker, 2003). To date, more than 55 classes of riboswitches have been identified that can sense a diverse range of ligands, including small metabolites, anions, cations, amino acids, and nucleotides (Breaker, 2022; McCown et al., 2017). Furthermore, riboswitches responding to the same ligands have been found to exhibit distinct consequences and structures. For instance, there are four types of guanidine riboswitches, namely guanidine-I, guanidine-II, guanidine-III, and guanidine-IV riboswitch, which specifically bind to guanidine. Notably, the guanidine-IV riboswitch differs significantly from other guanidine riboswitches (Battaglia & Ke, 2018; L. Huang et al., 2017; Lin Huang et al., 2017; Lenkeit et al., 2020; Nelson et al., 2017; Salvail et al., 2020). Specifically, the guanidine-IV riboswitch is able to enhance the transcription of *mepA* by forming an anti-terminator structure upon guanidine binding. This structure plays a crucial role in exporting guanidine and reducing its toxicity in cells, making the guanidine-IV riboswitch a potential target for antibiotics (Kermani et al., 2018). Although the atomic-resolution structures of the guanidine-IV riboswitch have not been solved, it is proposed that a kissing loop (KL) forms in the riboswitch in the presence of guanidine. This KL facilitates the dissociation of the terminator and promotes transcriptional read-through (Lenkeit et al., 2020; Salvail et al., 2020). KL or pseudoknot formation upon ligand binding is a common occurrence in various riboswitches, including adenine, guanine, ZTP, pre-Q1, fluoride, and c-di-AMP riboswitches (Jones & Ferre-D'Amare, 2017; Lenkeit et al., 2020; Salvail et al., 2020). However, the mechanism by which KL affects gene expression in a transcriptional riboswitch, particularly during transcription, remains elusive.

The folding of RNA during transcription plays a critical role in its function, especially in riboswitches involved in gene regulation. Previous studies have investigated the co-transcriptional folding of various riboswitches using different techniques. For instance, Frieda *et al.* employed the optical-trapping assay to examine the co-transcriptional folding of an adenine riboswitch at the single-molecule resolution (Frieda & Block, 2012). Helmling *et al.* and Binas *et al.*, on the other hand, used NMR to map the transcriptional intermediates of the

2′-deoxyguanosine (2′-dG) and ZMP riboswitches at the single-nucleotide resolution (Binas et al., 2020; Helmling et al., 2017). Landgraf *et al.* utilized NMR and computational modeling to identify the ligand-sensing transcriptional window for the c-di-GMP and c-GAMP riboswitches (Landgraf et al., 2022). Hua *et al.* investigated the co-transcriptional folding of the twister ribozyme and the ZTP riboswitch by mimicking the folding process using helicases to dissociate an RNA-DNA hybrid (Hua et al., 2020; Hua et al., 2018). Uhm *et al*., Widom *et al*., and Yadav *et al*. employed the single-molecule fluorescence resonance energy transfer (smFRET) strategy to study the co-transcriptional folding of the TPP, pre-Q1, and fluoride riboswitches by assembling transcriptional complexes (Uhm et al., 2018; Widom et al., 2018; Yadav et al., 2022). Xue *et al*. monitored the folding of a growing SAM-VI riboswitch at the single-molecule resolution by FRET (Xue et al., 2023). Despite these previous investigations, there is lack of information regarding the conformational changes and ligand-sensing behavior of the guanidine-IV riboswitch during transcription. In this study, we used position-specific labeling of RNA (PLOR) to introduce a FRET pair, Cy3 and Cy5, at sites 78 and 35, respectively. Subsequently, we examined the ligand and Mg^{2+} responses of the aptamer domain, terminator/anti-terminator, and full-length guanidine-IV riboswitch using smFRET. Our findings revealed that both guanidine and Mg^{2+} facilitated the formation of a KL in the aptamer domain and significantly increased the KL-formed conformation in that domain. Interestingly, unlike the aptamer domain, the addition of guanidine and Mg^{2+} only had a minimal effect on the formation of the KL-formed anti-terminator structure in the terminator/anti-terminator or full-length RNA. Additionally, we mimicked the conformational changes and ligand-sensing behavior from the aptamer domain to the terminator sequence of the guanidine-IV riboswitch during transcription using smFRET and PLOR. The formation of the KL increased as the riboswitch was transcribed up to 88 nucleotides (corresponding to the aptamer), but decreased as the riboswitch was transcribed from 88 to 105 nucleotides (corresponding to the terminator). Based on our data, it became evident that the transcriptional fate did not determined by the terminator sequence, but rather by the aptamer region, which exhibited distinct ligand-sensing abilities.

RESULTS

The construction and characteristics of the guanidine-IV riboswitch

The *Clostridium botulinum* guanidine-IV riboswitch was investigated in this study. The secondary structures of the guanidine-IV riboswitch are depicted in Figures 1A and 1B. In the absence of the guanidinium cation (Gua^+), the terminator consists of the aptamer domain (in black) and poly-U tail (in orange). This terminator is proposed to terminate transcription by dissociating RNA polymerase from the transcription system (Figure 1A). However, in the presence of Gua^+, the formation of a KL (in green, Figure 1B) hinders the formation of the complete terminator stem due to steric exclusion. This leads to the formation of the anti-terminator structure and subsequently activates the expression of its downstream genes (Figures 1C and 1D). The full-length riboswitch includes the nucleotides highlighted in blue, in addition to the terminator/anti-terminator region (orange, Figure 1B). In our study, we observed that the transcriptional read-through of the guanidine-IV riboswitch was responsive to Gua^+, with an apparent EC50 of approximately 68.7 μM (Figure 1D). This is comparable to the reported K_D of approximately 64 μM that was determined by in-line probing (Salvail et al., 2020). Higher read-through efficiencies were detected at higher Gua^+ concentrations, as presented in Figure 1D, consistent with previous findings (Lenkeit et al., 2020). In order to probe the structural changes of different domains in the guanidine-IV riboswitch under various conditions, we applied PLOR to introduce Cy3 and Cy5 at sites 78 and 35 in the aptamer (riboG-apt), terminator/anti-terminator (riboG-term), and full-length guanidine-IV riboswitch (riboG) . Sites 78 and 35 are close to the KL, making them suitable for monitoring the KL formation at different Mg^{2+} and Gua^+ concentrations.

smFRET revealed the significant effects of Mg^{2+} and Gua^+ on riboG-apt

smFRET is a powerful method that can detect multiple conformations by measuring the energy transfer efficiency (E_{FRET}) of a pair of fluorophores at the single molecule level. This technique has been extensively employed to investigate the conformational dynamics of RNA at the single-molecule level (Manz et al., 2017; Uhm et al., 2018). When the riboG-apt labeled with dual fluorophore-labeled (Figure 2A, Figure 2– figure supplement 1 and 2A) was examined, a single peak (E_{FRET} ~ 0.2) was observed in the presence of 0 mM Mg^{2+} and 0 mM Gua^+ (Figure 2B and Figure 2– figure supplement 2B). This peak is believed to correspond to the unfolded structure of riboG-apt, where the KL is not formed and thus, the labeled sites are distant from each other. Furthermore, in the presence of 2.0 mM Mg^{2+}, three peaks (E_{FRET} ~ 0.2, 0.5, and 0.8) were observed, as revealed by hidden Markov modeling

(Figure 2C). This suggests the coexistence of at least three structures when 2.0 mM Mg^{2+} is present, with the peak at an E_{FRET} of approximately 0.8 likely representing the structure involving the KL formation. In contrast, the peak with an E_{FRET} ~ 0.5 corresponded to a more compact structure compared to the unfolded structure, which we referred to as the pre-folded structure (Figure 2D). Notably, at 2.0 mM Mg^{2+}, these three states exhibited high dynamics, with transitions occurring particularly between the pre-folded and the unfolded states (Figures 2B and 2C). Our results demonstrate that the presence of Mg^{2+} induces a conformational change in the unfolded riboG-apt, leading to the adoption of more compact pre-folded and folded conformations. The proportion of the folded conformation significantly increased to approximately 90% at 20.0 mM Mg^{2+} (Figure 2E and Figure 2– figure supplement 2G). However, even with high concentrations of Mg^{2+}, riboG-apt remained flexible and dynamic in its transition between states (Figure 2E and Figure 2– figure supplement 2). The nucleotides surrounding the KL are crucial for its formation. Specifically, the G77C mutation has been found to significantly interfere with the KL formation, aligning with previous research (Lenkeit et al., 2020). Consistent with our expectations, the peaks corresponding to EFRET values of approximately 0.5 and 0.8 were not observed in our riboG-G77C variant, which contains the G77C mutation, even in the presence of a high Mg^{2+} concentration (50 mM; Figure 2– figure supplement 3). Our findings indicate that the G77C mutation disrupts the formation of the KL, consequently affecting the structures associated with E_{FRET} ~ 0.5 and 0.8. This observation strongly supports our hypothesis that the peak at E_{FRET} ~ 0.8 corresponds to the conformation folded with the KL.

In addition to Mg^{2+}, Gua^{+} also had the ability to promote the folded conformation (E_{FRET} ~ 0.8) of riboG-apt. However, Gua^{+} exhibited lower efficacy compared to Mg^{2+}, as evidenced by the proportion of the folded conformation being approximately 25% in the presence of 20.0 mM Gua^{+}. This value is significantly lower than the approximately 90% observed in the presence of 20.0 mM Mg^{2+} (Figure 2E, Figure 2– figure supplement 2G and 4F). Our observations also revealed that riboG-apt exhibited pronounced dynamics, frequently transiting among the three states at 10.0–100.0 mM Gua^{+} (Figure 2– figure supplement 4E–H). The presence of Mg^{2+} was critical in facilitating the induction of the folded state by Gua^{+}. Notably, riboG-apt showed increased susceptibility to Gua^{+} in the presence of Mg^{2+} (Figure 2F, Figure 2– figure supplement 5). Upon the addition of 0.5 mM Gua^{+} and 0.5 mM Mg^{2+}, the KL-folded conformation predominated in riboG-apt. The proportion of the KL-folded conformation increased to over 40%, which was comparable to

the effect observed with a 20-fold increase in Gua^+ in the absence of Mg^{2+} (Figure 2– figure supplement 4B and 5E). Interestingly, at 0.5 mM Mg^{2+}, Gua^+ bound to riboG-apt with a K_d of 286 μM (Figure 2– figure supplement 5H), higher than the K_d of 64 μM that was determined by in-line probing in the presence of 20 mM Mg^{2+} (Salvail et al., 2020). This difference is likely due to the low concentration of Mg^{2+}, which has a weak ability to help guanidine induced the KL conformation. In addition, we observed that riboG-apt became more stable as the concentration of Gua^+ increased, particularly in the presence of high Mg^{2+} (Figure 2– figure supplement 6). Surprisingly, the proportion of the folded conformation hardly increased when Mg^{2+} exceeded 2.0 mM in the presence of 1.0 mM Gua^+. Taking into account that Gua^+ was present in a positively charged state in the buffer employed for our FRET studies, we conducted additional experiments to investigate the impact of commonly used cations, including Na^+, K^+, and urea (a structural analog of guanidine). Interestingly, we observed minimal changes in the folded conformation of riboG-apt upon the addition of Na^+, K^+, or urea. These findings suggest that the effects of Gua^+ on the folded conformation are distinct from those of the tested cations. Furthermore, our results indicate that Gua^+ specifically binds to riboG-apt and induces structural changes as a ligand, rather than simply acting as a general cation or chaotrope (Figure 2G).

smFRET analysis revealed the slight effects of Mg^{2+} and Gua^+ on riboG-term and riboG

Unlike riboG-apt, riboG-term labeled with dual fluorophores (Figure 3A, Figure 3–figure supplement 1) exhibited the coexistence of three conformations, characterized by E_{FRET} values of approximately 0.2, 0.5, and 0.8. This coexistence was observed even in the absence of Mg^{2+} and Gua^+ (Figure 3B, Figure 3–figure supplement 2A and 2B). The sensitivity of RiboG-term to Gua^+ was significantly lower compared to riboG-apt. This is evidenced by the fact that, in the presence of 2.0 mM Mg^{2+}, the addition of 1.0 mM Gua^+ only resulted in a proportion of approximately 4% of the folded conformation for riboG-term, while it was approximately 60% for riboG-apt (Figures 2B and 3B). With the increase of either Mg^{2+} from 0 to 50.0 mM or Gua^+ from 0 to 100.0 mM, less than 12% of the molecules transited dynamically among the three states of riboG-term (Figure 3C, Figure 3–figure supplement 2 and 3). This finding suggests that the unfolded structure of riboG-term without KL (E_{FRET} ~ 0.2) is stable, and high concentrations of Mg^{2+} or Gua^+ only slightly affect the KL formation. In the presence of 0.5 mM Mg^{2+}, the structural change of riboG-term in response to increasing Gua^+ was negligible (Figure 3D, Figure 3–figure supplement 4). Surprisingly, in

the presence of 1.0 mM Gua^+, the conformation dynamics of riboG-term became more evident as Mg^{2+} increased. Moreover, at high Mg^{2+} concentrations, such as 10.0 mM, the abundance of the folded conformation (E_{FRET} ~ 0.8) significantly elevated with increasing Gua^+ (Figure 3E and Figure 3–figure supplement 5). This suggests that Gua^+ enhances the flexibility of riboG-term, potentially triggering its structural changes and facilitating the regulatory function of riboG in the presence of Mg^{2+}.

In the presence of Mg^{2+} and/or Gua^+, the FRET histogram of Cy3Cy5-riboG (Figures 4A and Figure 4–figure supplement 1) displayed a greater number of peaks compared to riboG-apt and riboG-term (Figures 4B and Figure 4–figure supplement 2). Additionally, the smFRET traces revealed structural transitions among the states, as shown in Figure 4–figure supplement 2–5. The presence of more structures in the full-length riboswitch compared to the aptamer domain is consistent with findings in other RNA molecules, such as the 2′-dG riboswitch (Helmling et al., 2017). Notably, upon the addition of 1.0 mM Gua^+ in the presence of 2.0 mM Mg^{2+}, the proportion of the new peak (E_{FRET} ~ 0.4) increased from 19% to 29%, and then decreased as the Mg^{2+} concentrations increased from 2 to 10 mM (Figure 4–figure supplement 2D and 4B–D). The addition of 0–50.0 mM Mg^{2+} or 0–100 mM Gua^+ only slightly altered the proportion of the folded conformation (E_{FRET} ~ 0.8) of riboG (Figure 4C, 4D, Figure 4–figure supplement 2 and 3). Even in the presence of 1.0 mM Gua^+, an increase in Mg^{2+} concentration from 0 to 10.0 mM had little effect on the proportion of the folded conformation (Figure 4–figure supplement 3B and 4B–D). However, the effect of Gua^+ on riboG in the presence of 10.0 mM Mg^{2+} was significantly more pronounced compared to its effect in the absence of Mg^{2+} (Figure 4C and Figure 4–figure supplement 5B–F). The impact of Mg^{2+} and Gua^+ on the folded conformation of riboG showed similarities to their effects on riboG-term but had distinct differences compared to their effects on riboG-apt (Figures 4D and 4E). Overall, the effects of Mg^{2+} and Gua^+ on the structures of riboG and riboG-term were weaker compared to their effects on riboG-apt.

Kinetic analysis of smFRET data to identify the folding pathway of the guanidine-IV riboswitch

The guanidine-IV riboswitch exhibits dynamic behavior, with its structural transitions in response to Mg^{2+} and Gua^+ closely linked to transcription termination. The relative free energy ($\Delta\Delta G$) was calculated based on the state populations in the FRET histogram (Figures 5A and 5B). For riboG-apt, both the pre-folded and folded states displayed higher $\Delta\Delta G$

values compared to the unfolded state, indicating that the former states were less stable in the presence of 2.0 mM Mg^{2+}. However, the addition of 1 mM Gua^{+} successfully reduced the *ΔΔG* of the folded state to a level lower than that of the unfolded state (Figure 5A). Meanwhile, only slight decreases in *ΔΔG* were observed for riboG-term and riboG upon the addition of 1.0 mM Gua^{+} in the presence of 2.0 mM Mg^{2+} (Figure 5B). The dwell time distributions were obtained from the single-molecule trajectories of FRET data for riboG-apt, riboG-term, and riboG (Figures, 5C–E and Figure 5–figure supplement 1–4). The exponential decays of the dwell time were fitted to a first-order kinetic equation, allowing for the determination of dwell time and rate constants for the individual states of riboG-apt (Figures 5C–E). Based on these results, we proposed folding pathways to illustrate the transcriptional fate of the guanidine-IV riboswitch under different conditions (Figure 5F and Figure 5–figure supplement 4). The analysis of the dwell time data from single-molecule trajectories indicated that the folding process of riboG-apt was influenced by Mg^{2+} and/or Gua^{+}. In the presence of 2.0 mM Mg^{2+}, there was inefficient structural switching from the unfolded riboG-apt ($\tau \approx 0.7$ s) to the pre-folded state ($\tau \approx 0.11$ s) or folded riboG-apt ($\tau \approx 0.4$ s), resulting in the production of the terminator during transcription (red arrows, Figure 5F). Conversely, in the presence of 1.0 mM Gua^{+}, the primary switching of riboG-apt occurred between the unfolded ($\tau \approx 0.6$ s) and folded states ($\tau \approx 1.04$ s), which can subsequently be transcribed into the anti-terminator (blue arrows, Figure 5F).

smFRET analysis revealed the Gua^{+}-sensitive transcription window of riboG

The sensitivity of Gua^{+} varied among the post-transcriptional riboG-apt, riboG-term, and riboG sequences. The folding and interactions of RNA during transcription play a critical role in its control functions for transcriptional riboswitch. To mimick how nascent riboG responds to Gua^{+} and its regulatory effects during transcription, we utilized PLOR to control its transcription at a single-nucleotide pace, Simultaneously, we collected smFRET data from active transcription elongation complexes (ECs) containing nascent RNA of different lengths (Figures 6A, 6B and Figure 6–figure supplement 1). PLOR is a liquid–solid hybrid phase transcription process that allows for pausing transcription at specific positions by omitting certain nucleotide triphosphates (NTPs). This paused transcription can then be restarted by adding the necessary NTPs. This unique “pause–restart” transcriptional mode enables the evaluation of instant changes in the environment, such as the addition or removal of Gua^{+} at specific steps, facilitating the monitoring of nascent RNA under varied conditions. To

investigate the range of ligand-responsiveness in riboG, we employed PLOR to generate various transcriptional complexes with different RNA lengths, this allowed us to assess the impact of Gua^+ on the guanidine-IV riboswitch throughout the transcription process. We monitored the behavior of active transcription complexes containing guanidine-IV riboswitches with varying lengths of 87 to 105 nucleotides (nt) using smFRET (Figures 6C–I and Figure 6–figure supplement 2–6). To distinguish between the different complexes, we named them based on their nucleotide length, for example, the EC-87 for the 87 nt complex. We collected smFRET histograms for EC-87, EC-88, EC-89, EC-91, EC-94, EC-96, and EC-105 in the presence of 0.5 mM Mg^{2+} and either 0 or 10.0 mM Gua^+ (Figures 6C–I and Figure 6–figure supplement 2–4). Three distinct peaks ($E_{FRET} \approx 0.2$, 0.5, and 0.8) were observed, with the high-FRET peak suggesting the presence of a newly folded RNA structure, potentially containing a KL, as the transcript size exceeded 87 nt. In the presence of 0.5 mM Mg^{2+}, the proportion of the folded structure slightly decreased during transcription from 87 to 88 nt (from approximately 15% to 13%), but then sharply decreased to 3% at 89 nt. The addition of Gua^+ significantly increased the proportion of the folded state for EC-88 compared to EC-87. For longer ECs, such as EC-89, EC-91, and EC-94, the proportion of the folded state remained relatively stable, with only a few molecule traces between the unfolded and folded states (Figures 6E–I, Figure 6–figure supplement 3–4). At 0.5, 2.0, and 6.0 mM Mg^{2+}, the proportions of the peaks changed differently, but EC-88 exhibited more dramatic changes than other ECs upon the addition of Gua^+ (Figure 6J and Figure 6–figure supplement 2–7). These results suggest that the optimal formation of KL occurs during transcription of the 88 nt nascent RNA, and a drastic structural switch takes place between 88 and 89 nt in the presence of Mg^{2+}. Interestingly, the addition of 1.0 mM Gua^+ induced more pronounced changes in the majority of ECs at higher Mg^{2+} concentrations (Figure 6J and Figure 6–figure supplement 5–6). These findings suggest that the ECs exhibit a greater propensity for structural transitions upon the addition of Gua^+ at high Mg^{2+} concentrations. Furthermore, under conditions of 0.5 mM Mg^{2+} and 10.0 mM Gua^+, the proportions of folded structures ($E_{FRET} \sim 0.8$) in EC-88 and EC-105 were approximately 36% and 14% lower, respectively, compared to those observed in the isolated post-transcriptional riboG-apt and riboG-term (Figures 6D, 6I, Figure 2–figure supplement 4G and Figure 3–figure supplement 4F). These results suggest that the interactions between nascent RNA and DNA templates or RNA polymerase (RNAP) can hinder the folding of the RNA. Additionally, our collected eluent

was active elongation complex, as evidenced by the production of full-length and terminated transcripts when NTPs were added to the eluent in the elongation assay (Figure 6K).

Gua^+ modulated the transcription of the guanidine-IV riboswitch at specific sequences

To investigate the regulatory functions of the nascent riboswitch at different lengths during transcription, we performed a transcriptional termination assay of the guanidine-IV riboswitch using PLOR (Figure 7A and Figure 7–figure supplement 1). Specifically, we carefully designed eight PLOR experiments to temporarily pause the transcription at nucleotides 69, 77, 78, 83, 88, 91, 94 and 105, respectively, before transcribing the remaining RNA fragment in the last step, following strategies 1–8 (Figures 7B, 7C and Figure 7–figure supplement 1B). In the absence of Gua^+, there was minimal change in transcriptional termination among strategies 1–7, but a sharp decrease of approximately 20% was observed for strategy 8 (Figure 7–figure supplement 1C and 1D). However, with the addition of Gua^+ in the last step, there was littler variation in transcriptional read-through of the guanidine-IV riboswitch among strategies 1–5, but a gradual decrease was observed from strategy 6 to strategy 8. Notably, there was a dramatic decrease in anti-termination from strategy 5 to strategy 8 (Figure 7–figure supplement 1C and 1D). Furthermore, we observed a significant increase in read-through upon the addition of Gua^+ in our single-round transcription reactions when the RNA length reached 88 nt (Figure 7D). Additionally, a slight increase in read-through was observed at the pausing site 105, which is consistent with the smFRET data presented in Figure 6J. This indicates that Gua^+ can still bind and induce slight structural changes in the guanidine-IV riboswitch, even if its full terminator sequence has been transcribed. Our findings from *in vitro* transcriptional termination assays and smFRET results, indicating that EC-91 exhibits a more stable fold with a longer stem, making it less sensitive to environmental changes compared to EC-88 (Figures 6F and 7D).

DISCUSSION

In this study, we have demonstrated that both Mg^{2+} and Gua^+ play critical roles in promoting structural folding and transcriptional anti-termination in guanidine-IV riboswitches. Based on our findings, we propose a model illustrating the termination/anti-termination process of the guanidine-IV riboswitch as transcription progresses (Figure 8). In the presence of Mg^{2+}, the proportion of the anti-terminator induced by Gua^+ increases as transcription progresses up to

EC-88. However, after EC-88 a significant decrease is observed up to EC-105 (Figures 6 and 8). The elongation of transcriptional from EC-88 to EC-105 leads to impaired KL formation and an increase in terminator abundance. This incremental switch from the anti-terminator to the terminator from EC-88 to EC-105 is influenced by the elongating P2 structure (Figure 8). The competition between the P2 and KL structures determines the proportions of the terminator and the anti-terminator in the guanidine-IV riboswitch. The stability of the terminator is enhanced by the presence of P2, and the increase in base pairs within P2 strengthens the terminator as transcription proceeds (highlighted in orange, Figure 8). On the other hand, the stability of the anti-terminator is dependent on the formation of KL. The elongation of P2 shortens the flexible linker between P1 and P2, which creates steric hindrance for KL after EC-88. Furthermore, the addition of Gua^+ facilitates the functional switch from the terminator to the anti-terminator for constructs ranging from EC-87 to EC-105. However, we propose a narrow Gua^+-sensitive transcription window for the guanidine-IV riboswitch, with a dramatic switch observed during the extension from EC-87 to EC-88 upon Gua^+ addition (shown in a green box, Figure 8). It is worth noting that the ligand-sensitive sequence for the guanidine-IV riboswitch is located within the aptamer domain, spanning 88 nucleotides.

Our findings demonstrate that the guanidine-IV riboswitch possesses a distinct binding window that can be modulated by guanidine. The mechanism of anti-termination supports a model in which the formation of a long-range KL prevents the assembly of a rigid terminator. This distinguishes the guanidine-IV riboswitch from typical transcriptional riboswitches that rely on overlapping sequences and base-pair rearrangements for functional change (Strobel et al., 2019; Yadav et al., 2022; Zhao et al., 2017). Moreover, our results reveal the existence of at least three distinct states in the guanidine-IV riboswitch, including a folded state characterized by the presence of a KL that plays a critical role in ligand binding and transcriptional regulation. Importantly, the formation of the long-range KL in the aptamer domain is specifically responsive to guanidine, as other cations such as K^+, Na^+, and urea do not produce the same effect. While guanidine contributes to structural switching in the aptamer domain, its impact on the terminator or full-length guanidine-IV riboswitch is comparatively weak. Additionally, our data indicate that guanidine induces less significant changes once the RNA polymerase has transcribed the aptamer domain. Kinetic analysis reveals that the addition of guanidine leads to a slight decrease in the dwell time of the unfolded state of the aptamer domain but a significant increase in the dwell time of the folded

state containing a KL. This facilitates the structural transition from the unfolded state to the folded state, ultimately promoting transcriptional read-through.

In the transcriptional mimicking assay, the nascent RNA displayed a weaker response to guanidine compared to the post-transcriptional counterparts. This suggests that in the guanidine-IV riboswitch system, the DNA templates and RNA polymerase play a role in RNA folding and guanidine binding, in line with the previous findings for the pre-Q1 and SAM-VI riboswitches (Widom et al., 2018; Xue et al., 2023). Moreover, the guanidine sensitivity of EC-87 indicates that guanidine regulation for the guanidine-IV riboswitch occurs before transcription of the aptamer domain is completed. Additionally, the sensitivity to guanidine gradually increases in the RNA within ECs until EC-88, after which it decreases. In other words, there exhibits a limited transcriptional window for the guanidine-IV riboswitch to dynamically respond to guanidine, and the inclination to form the terminator increases after transcribing 88 nucleotides, resulting in a decrease in the abundance of the KL-folded conformation. This aligns with previous findings that the transcription decision of a transcriptional riboswitch is made prior to terminator formation (Sherwood & Henkin, 2016; Wickiser et al., 2005). However, our data also suggest that guanidine can induce slight structural changes in the guanidine-IV riboswitch even after the terminator domain has been transcribed and stabilized. Similar observations have been reported for other riboswitches, although the transcriptional window sensitive to the ligand differs among riboswitches (Wickiser et al., 2005).

MATERIAL AND METHODS

DNA template preparation

The biotin labeled DNA templates were prepared by PCR as described earlier (Liu et al., 2018; Liu et al., 2015). The sequences of the DNA templates are listed in Supplementary Table S1. The primers used in PCR were ordered from Sangon Biotech (Shanghai, China). The DNA products generated from PCR were purified by 12% denaturing PAGE (polyacrylamide electrophoresis) before immobilized on streptavidin-coated agarose beads (Smart-Life Science, Changzhou, China) in the buffer (40 mM Tris-HCl, 100 mM K_2SO_4, 6 mM $MgSO_4$, pH 8.0) as described earlier (Liu et al., 2018). The solid-phase DNA templates were stored at 4 °C before usage.

Cy3Cy5-labeled riboG-apt, riboG-term and riboG synthesis

The Cy3Cy5-labeled RNA used in smFRET were synthesized by PLOR as described earlier (Liu et al., 2018; Liu et al., 2015). The schemes and reagents of synthesis of Cy3Cy5-riboG-apt, Cy3Cy5-riboG-term and Cy3Cy5-riboG are listed in Supplementary Tables S2, S3 and S4. For Cy3Cy5-riboG-apt synthesis, 10 μM DNA-beads gently shook with 10 μM T7 RNAP, 0.96 mM ATP, 0.96 mM GTP and 96 μM UTP in the buffer (40 mM Tris-HCl, 100 mM K_2SO_4, 6 mM $MgSO_4$, 10 mM DTT, pH 8.0) at 37 °C for 15 min in the first step. The reaction mixture was filtered by solid-phase extraction and rinsed for 3~4 times in the buffer (40 mM Tris-HCl, 6 mM $MgSO_4$, pH 8.0). And the bead-rinsing procedure was performed before the addition of NTPs in each step except noted. The residual steps were proceeded in the elongation buffer (40 mM Tris-HCl, 6 mM $MgSO_4$, 10 mM DTT, pH 8.0) at 25 °C for 10 min with the addition of different NTP mixture at individual step as listed in Supplementary Table S2. The Cy3Cy5-labeled riboG-apt was collected at the last step, purified by 12% denaturing PAGE and reversed phase HPLC loaded with C8 column (4.6*250 mm, Cat. No. EXL-122-2546U, Phenomenex Luna, USA) as described earlier. The Cy3Cy5-riboG-term and Cy3Cy5-riboG were synthesized as Cy3Cy5-riboG-apt except different NTPs were added. The purified RNA was stored at -80 °C before usage.

Preparation of transcription complexes containing RNA at different lengths

The RNA sequences in the transcription complexes (ECs) are listed in Supplementary Table S5, and the ECs were collected at different steps of PLOR as listed in Supplementary Table

S6. For example, EC-87 was obtained as the following procedures: took 10 μL 10 μM DNA-beads from 200 μL of the PLOR reaction at step 14 and incubated with 1 μL 1 mM biotin at 25 °C for 20 min. The addition of biotin was to displace the biotin-labeled DNA template on the streptavidin-labeled beads, filtered by solid-phase exchange and collected the elution containing EC-87. EC-88, 89, 91, 94, 96 and 105 were obtained at steps15, 16, 17, 18, 20 and 21 similarly as EC-87 (Supplementary Table S6).

smFRET experiments and data analysis

0.5 μM Cy3Cy5-riboG-apt, Cy3Cy5-riboG-term or Cy3Cy5-riboG were hybridized with 0.75 μM biotinylated 13 nt-DNA by incubating at 90 °C for 5 min and then cooled to room temperature in the T50 buffer (10 mM Tris-HCl, 50 mM NaCl, pH 8.0). The sequence of the biotinylated DNA is listed in Supplementary Table S1. The hybridized Cy3Cy5-labeled RNA was then diluted to 10~100 pM for the subsequent smFRET measurements. Polymer-coated quartz slides were immersed at the 0.1 mg/μL biotin-PEG and 0.3 mg/μL m-PEG for 2 h (Roy et al., 2008), then coated with 0.2 mg/mL streptavidin for 5 min. 10~100 pM Cy3Cy5-labeled RNA or ECs in the buffer (10 mM Tris-HCl, 50 mM NaCl, 0~100 mM guanidine, 0~100 mM Mg^{2+}) was injected and then rinsed 3 times to remove the free RNA or ECs. 3 mM Trolox (MCE, USA), 5 mM 3,4-protocatechuic acid (PCA, Shanghai Aladdin Bio-Chem Technology Co., China) and 5 nM protocatechuate dioxygenase (PCD) was added to reduce the photobleaching (Aitken et al., 2008). smFRET experiments were performed by using an objective-type total internal reflection fluorescence (TRIF) microscopy and an inverted microscope (Eclipse Ti, Nikon, Japan) at 20 °C, with FRET marker dyes Cy3 (donor) and Cy5 (acceptor) was excited by 532 nm and 640 nm laser, respectively. Open-sourced software iSMS (Preus et al., 2015) was used to process the single-molecule videos to extract the time-dependent signals. Single-molecule trajectories were identified by Deep FRET (Thomsen et al., 2020). The FRET efficiency, E_{FRET} was calculated using the equation:

$$E_{FRET} = I_A/(I_A+I_D).$$

Where I_A and I_D are acceptor and donor fluorescence intensity, respectively. We used empirical Bayesian method of the hidden Markov modelling (HMM) package vbFRET to estimate the FRET states and the time points of transitions (Bronson et al., 2009). The transition density plots (TDP) were plotted by Python module matplotlib, and the lifetimes were plotted in histogram and fitted with a simple exponential decay function by Origin 8.5

to obtain the rate constants. The relative free energy, $\Delta\Delta G$ was measured using the equation $\Delta\Delta G_{ab} = -RT \ln(P_b/P_a)$, where R, T, P_a and P_b are the gas constant, absolute temperature, population of the observed state b and population of the control state a, respectively (Manz et al., 2017).

In vitro transcription termination assay

The single-round transcription termination assay was carried out by PLOR (Chien et al., 2023). The detailed procedure and reagents are listed in Supplementary Tables S7–15. 0~10 mM guanidine and 2~6 mM Mg^{2+} were added at step 8 in Supplementary Tables S7 to measure the effect of guanidine on transcription read-through of the guanidine-IV riboswitch. The products collected at the last step were loaded to 12% denaturing PAGE to compare the transcription read-through efficiencies at different conditions.

Acknowledgements

The work was supported by the National Key Research and Development Program of China [grant no. 2021YFA0910300] and National Natural Science Foundation of China [grant no. 32071300].

Author Contributions

L.G. and Y.L. designed experiments; L.G. collected and analyzed the FRET data; L.G. and D.C. collected *in vitro* data; L.G. and Y.L. drafted the manuscript and all authors contributed to the revision.

Competing Interests

The authors declare no competing interests.

Reference

1. Aitken, C. E., Marshall, R. A., & Puglisi, J. D. (2008). An oxygen scavenging system for improvement of dye stability in single-molecule fluorescence experiments. *Biophys J*, *94*(5), 1826-1835. https://doi.org/10.1529/biophysj.107.117689
2. Battaglia, R. A., & Ke, A. (2018). Guanidine-sensing riboswitches: How do they work and what do they regulate? *Wiley Interdiscip Rev RNA*, *9*(5), e1482. https://doi.org/10.1002/wrna.1482
3. Binas, O., Schamber, T., & Schwalbe, H. (2020). The conformational landscape of transcription intermediates involved in the regulation of the ZMP-sensing riboswitch from Thermosinus carboxydivorans. *Nucleic Acids Res*, *48*(12), 6970-6979. https://doi.org/10.1093/nar/gkaa427
4. Breaker, R. R. (2022). The Biochemical Landscape of Riboswitch Ligands. *Biochemistry*, *61*(3), 137-149. https://doi.org/10.1021/acs.biochem.1c00765
5. Bronson, J. E., Fei, J., Hofman, J. M., Gonzalez, R. L., & Wiggins, C. H. (2009). Learning Rates and States from Biophysical Time Series: A Bayesian Approach to Model Selection and Single-Molecule FRET Data. *Biophysical Journal*, *97*(12), 3196-3205. https://doi.org/10.1016/j.bpj.2009.09.031
6. Chien, P.-Y., Gao, L., & Liu, Y. (2023). Quantitative Analysis of Transcription Termination via Position-Selective Labeling of RNA (PLOR) Method. *International Journal of Molecular Sciences*, *24*(5). https://doi.org/10.3390/ijms24054934
7. Frieda, K.L., & Block, S.M. (2012).Direct Observation of Cotranscriptional Folding in an Adenine Riboswitch.Science, *338*, 397-400. https://doi.org/10.1126/science.1225722
8. Garst, A. D., Edwards, A. L., & Batey, R. T. (2011). Riboswitches: structures and mechanisms. *Cold Spring Harb Perspect Biol*, *3*(6). https://doi.org/10.1101/cshperspect.a003533
9. Helmling, C., Wacker, A., Wolfinger, M. T., Hofacker, I. L., Hengesbach, M., Furtig, B., & Schwalbe, H. (2017). NMR Structural Profiling of Transcriptional Intermediates Reveals Riboswitch Regulation by Metastable RNA Conformations. *J Am Chem Soc*, *139*(7), 2647-2656. https://doi.org/10.1021/jacs.6b10429
10. Hua, B., Jones, C. P., Mitra, J., Murray, P. J., Rosenthal, R., Ferre-D'Amare, A. R., & Ha, T. (2020). Real-time monitoring of single ZTP riboswitches reveals a complex and kinetically controlled decision landscape. *Nature Communications*, *11*(1), 4531. https://doi.org/10.1038/s41467-020-18283-1
11. Hua, B., Panja, S., Wang, Y., Woodson, S. A., & Ha, T. (2018). Mimicking Co-Transcriptional RNA Folding Using a Superhelicase. *J Am Chem Soc*, *140*(32), 10067-10070. https://doi.org/10.1021/jacs.8b03784
12. Huang, L., Wang, J., & Lilley, D. M. J. (2017). The Structure of the Guanidine-II Riboswitch. *Cell Chem Biol*, *24*(6), 695-702 e692. https://doi.org/10.1016/j.chembiol.2017.05.014
13. Huang, L., Wang, J., Wilson, T. J., & Lilley, D. M. J. (2017). Structure of the Guanidine III Riboswitch. *Cell Chemical Biology*, *24*(11), 1407-1415.e1402. https://doi.org/10.1016/j.chembiol.2017.08.021
14. Jones, C. P., & Ferre-D'Amare, A. R. (2017). Long-Range Interactions in Riboswitch Control of Gene Expression. *Annu Rev Biophys*, *46*, 455-481. https://doi.org/10.1146/annurev-biophys-070816-034042
15. Kavita, K., & Breaker, R. R. (2023). Discovering riboswitches: the past and the future. *Trends Biochem Sci*, *48*(2), 119-141. https://doi.org/10.1016/j.tibs.2022.08.009
16. Kermani, A. A., Macdonald, C. B., Gundepudi, R., & Stockbridge, R. B. (2018). Guanidinium export is the primal function of SMR family transporters. *Proc Natl Acad Sci U S A*, *115*(12), 3060-3065. https://doi.org/10.1073/pnas.1719187115
17. Landgraf, T., Volklein, A. E., Furtig, B., & Schwalbe, H. (2022). The cotranscriptional folding landscape for two cyclic di-nucleotide-sensing riboswitches with highly homologous aptamer domains acting either as ON- or OFF-switches. *Nucleic Acids Res*, *50*(12), 6639-6655. https://doi.org/10.1093/nar/gkac514
18. Lenkeit, F., Eckert, I., Hartig, J. S., & Weinberg, Z. (2020). Discovery and characterization of a fourth class of guanidine riboswitches. *Nucleic Acids Res*, *48*(22), 12889-12899. https://doi.org/10.1093/nar/gkaa1102
19. Liu, Y., Holmstrom, E., Yu, P., Tan, K., Zuo, X., Nesbitt, D. J., Sousa, R., Stagno, J. R., & Wang, Y. X. (2018). Incorporation of isotopic, fluorescent, and heavy-atom-modified nucleotides into RNAs by position-selective labeling of RNA. *Nat Protoc*, *13*(5), 987-1005. https://doi.org/10.1038/nprot.2018.002

20. Liu, Y., Holmstrom, E., Zhang, J., Yu, P., Wang, J., Dyba, M. A., De, C., Ying, J., Lockett, S., Nesbitt, D. J., Ferré-D'Amaré, A. R., Sousa, R., Stagno, J. R., & Wang, Y.-X. (2015). Synthesis and applications of RNAs with position-selective labelling and mosaic composition. *Nature*, *522*(7556), 368-372. https://doi.org/10.1038/nature14352
21. Mandal, M., & Breaker, R. R. (2004). Gene regulation by riboswitches. *Nat Rev Mol Cell Biol*, *5*(6), 451-463. https://doi.org/10.1038/nrm1403
22. Manz, C., Kobitski, A. Y., Samanta, A., Keller, B. G., Jaschke, A., & Nienhaus, G. U. (2017). Single-molecule FRET reveals the energy landscape of the full-length SAM-I riboswitch. *Nat Chem Biol*, *13*(11), 1172-1178. https://doi.org/10.1038/nchembio.2476
23. McCown, P. J., Corbino, K. A., Stav, S., Sherlock, M. E., & Breaker, R. R. (2017). Riboswitch diversity and distribution. *Rna*, *23*(7), 995-1011. https://doi.org/10.1261/rna.061234.117
24. Nelson, J. W., Atilho, R. M., Sherlock, M. E., Stockbridge, R. B., & Breaker, R. R. (2017). Metabolism of Free Guanidine in Bacteria Is Regulated by a Widespread Riboswitch Class. *Mol Cell*, *65*(2), 220-230. https://doi.org/10.1016/j.molcel.2016.11.019
25. Preus, S., Noer, S. L., Hildebrandt, L. L., Gudnason, D., & Birkedal, V. (2015). iSMS: single-molecule FRET microscopy software. *Nat Methods*, *12*(7), 593-594. https://doi.org/10.1038/nmeth.3435
26. Roy, R., Hohng, S., & Ha, T. (2008). A practical guide to single-molecule FRET. *Nat Methods*, *5*(6), 507-516. https://doi.org/10.1038/nmeth.1208
27. Salvail, H., Balaji, A., Yu, D., Roth, A., & Breaker, R. R. (2020). Biochemical Validation of a Fourth Guanidine Riboswitch Class in Bacteria. *Biochemistry*, *59*(49), 4654-4662. https://doi.org/10.1021/acs.biochem.0c00793
28. Serganov, A., & Nudler, E. (2013). A decade of riboswitches. *Cell*, *152*(1-2), 17-24. https://doi.org/10.1016/j.cell.2012.12.024
29. Sherlock, M. E., & Breaker, R. R. (2020). Former orphan riboswitches reveal unexplored areas of bacterial metabolism, signaling, and gene control processes. *Rna*, *26*(6), 675-693. https://doi.org/10.1261/rna.074997.120
30. Sherwood, A. V., & Henkin, T. M. (2016). Riboswitch-Mediated Gene Regulation: Novel RNA Architectures Dictate Gene Expression Responses. *Annu Rev Microbiol*, *70*, 361-374. https://doi.org/10.1146/annurev-micro-091014-104306
31. Strobel, E. J., Cheng, L., Berman, K. E., Carlson, P. D., & Lucks, J. B. (2019). A ligand-gated strand displacement mechanism for ZTP riboswitch transcription control. *Nat Chem Biol*, *15*(11), 1067-1076. https://doi.org/10.1038/s41589-019-0382-7
32. Thomsen, J., Sletfjerding, M. B., Jensen, S. B., Stella, S., Paul, B., Malle, M. G., Montoya, G., Petersen, T. C., & Hatzakis, N. S. (2020). DeepFRET, a software for rapid and automated single-molecule FRET data classification using deep learning. *eLife*, *9*. https://doi.org/10.7554/eLife.60404
33. Uhm, H., Kang, W., Ha, K. S., Kang, C., & Hohng, S. (2018). Single-molecule FRET studies on the cotranscriptional folding of a thiamine pyrophosphate riboswitch. *Proc Natl Acad Sci U S A*, *115*(2), 331-336. https://doi.org/10.1073/pnas.1712983115
34. Wickiser, J. K., Winkler, W. C., Breaker, R. R., & Crothers, D. M. (2005). The speed of RNA transcription and metabolite binding kinetics operate an FMN riboswitch. *Mol Cell*, *18*(1), 49-60. https://doi.org/10.1016/j.molcel.2005.02.032
35. Widom, J. R., Nedialkov, Y. A., Rai, V., Hayes, R. L., Brooks, C. L., 3rd, Artsimovitch, I., & Walter, N. G. (2018). Ligand Modulates Cross-Coupling between Riboswitch Folding and Transcriptional Pausing. *Mol Cell*, *72*(3), 541-552 e546. https://doi.org/10.1016/j.molcel.2018.08.046
36. Winkler, W. C., & Breaker, R. R. (2003). Genetic control by metabolite-binding riboswitches. *Chembiochem*, *4*(10), 1024-1032. https://doi.org/10.1002/cbic.200300685
37. Xue, Y., Li, J., Chen, D., Zhao, X., Hong, L., & Liu, Y. (2023). Observation of structural switch in nascent SAM-VI riboswitch during transcription at single-nucleotide and single-molecule resolution. *Nature Communications*, *14*(1). https://doi.org/10.1038/s41467-023-38042-2
38. Yadav, R., Widom, J. R., Chauvier, A., & Walter, N. G. (2022). An anionic ligand snap-locks a long-range interaction in a magnesium-folded riboswitch. *Nature Communications*, *13*(1), 207. https://doi.org/10.1038/s41467-021-27827-y
39. Zhao, B., Guffy, S. L., Williams, B., & Zhang, Q. (2017). An excited state underlies gene regulation of a transcriptional riboswitch. *Nat Chem Biol*, *13*(9), 968-974. https://doi.org/10.1038/nchembio.2427

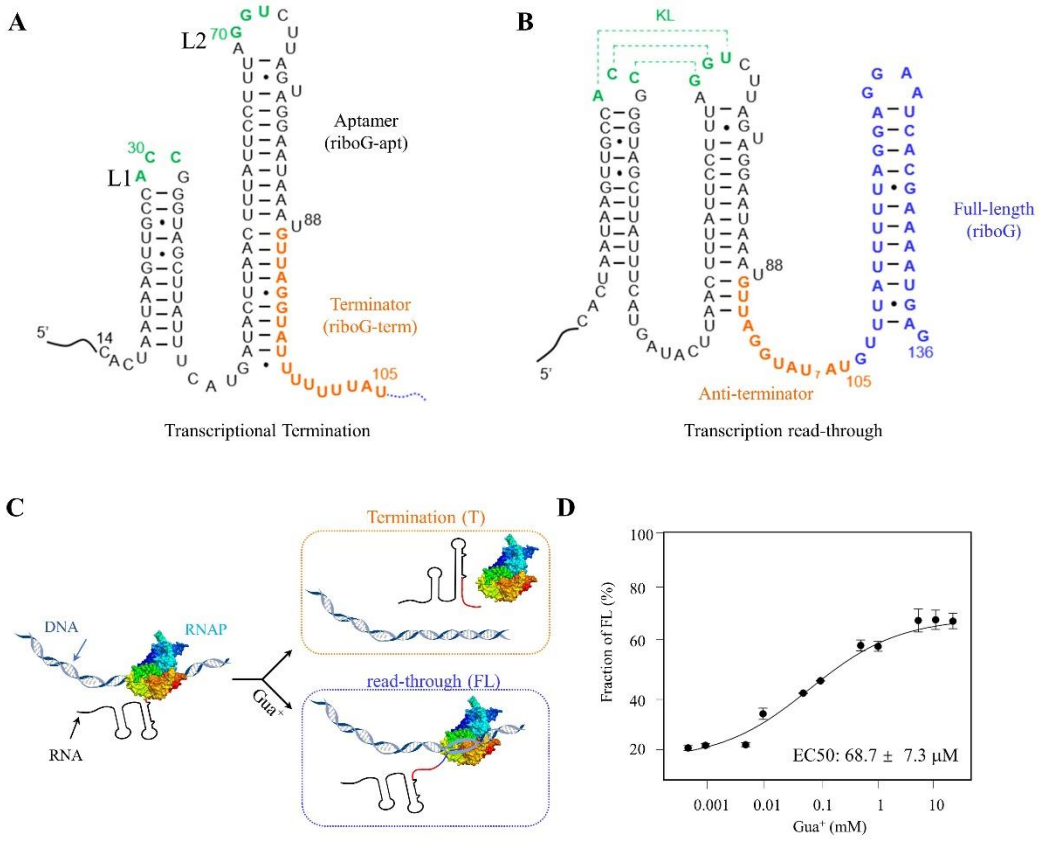

Figure 1. Characteristics of the *C. botulinum* guanidine-IV riboswitch. (A, B) The secondary structures of the transcriptional termination and read-through states of the guanidine-IV riboswitch. The full-length of the guanidine-IV riboswitch contains the aptamer domain (black), terminator (orange) and the extended sequence (blue). The green nucleotides are involved in forming a KL in the anti-terminator state. (C) A transcriptional model of the guanidine-IV riboswitch. The DNA is shown in blue ribbons. The colors in the RNA are encoded as in (A) and (B). And the addition of Gua^+ facilitates transcription read-through. (D) The percentages of the transcription read-through plotted with 0.5 μM–20.0 mM Gua^+ at 6.0 mM Mg^{2+} in the three independent transcription termination reactions.

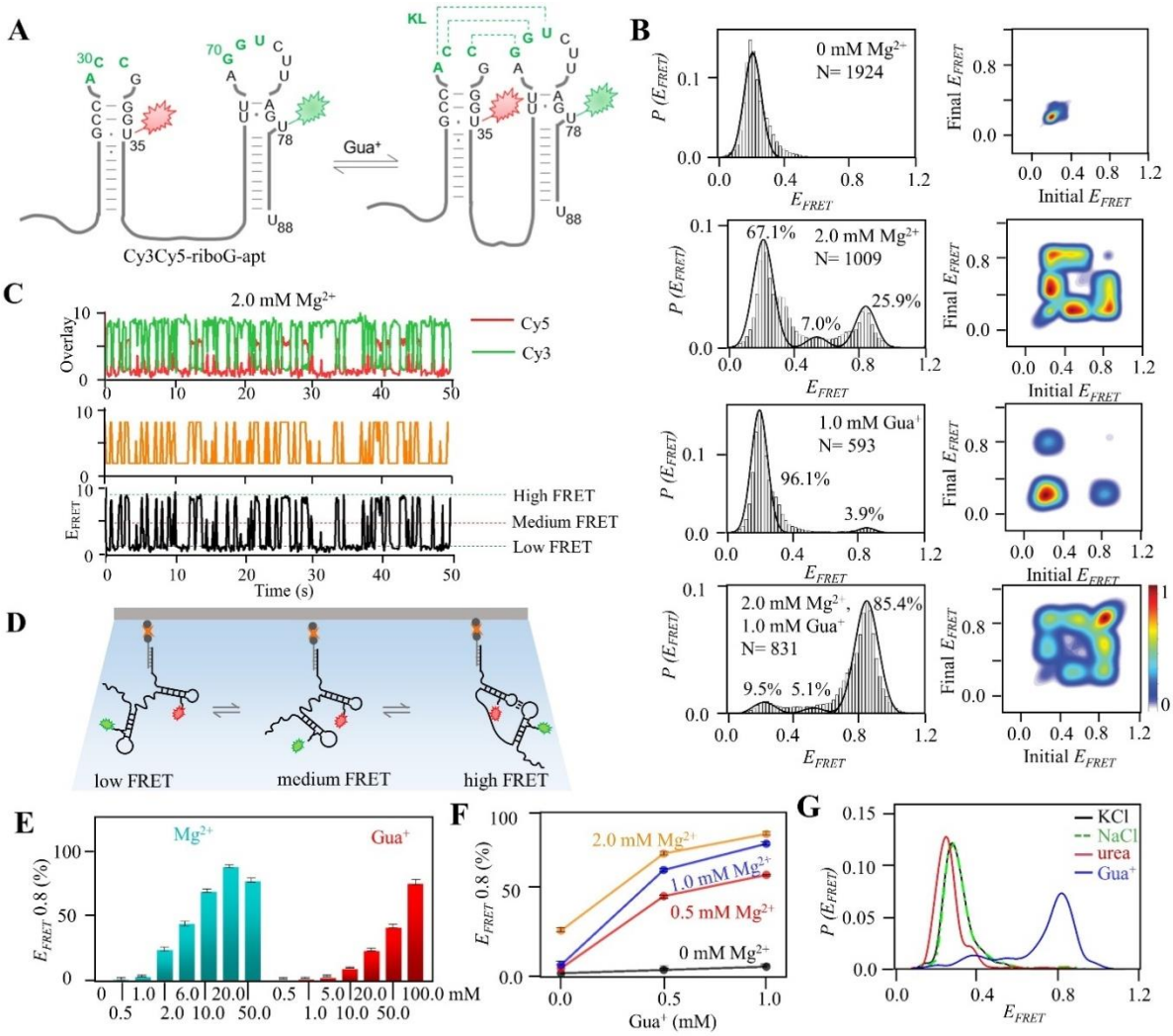

Figure 2. smFRET studies of post-transcriptional Cy3Cy5-riboG-apt at different concentrations of Mg^{2+} and Gua^{+}. (A) The secondary structures of Cy3Cy5-riboG-apt at the unfolded (left) and the folded state (right). Cy3 and Cy5 are shown by green and red sparkles, respectively. (B) smFRET histograms and transition density plots for Cy3Cy5-riboG-apt at 0 mM Mg^{2+}, at 2.0 mM Mg^{2+}, at 1.0 mM Gua^{+}, and at 2.0 mM Mg^{2+} and 1.0 mM Gua^{+}. (C) HMM analysis of smFRET time trace of Cy3Cy5-riboG-apt at 2.0 mM Mg^{2+}, the time resolution is 0.1s. (D) Schematic diagram for three conformations of Cy3Cy5-labeled RNA in smFRET experiments. The Cy3Cy5-labeled RNA is hybridized with a biotinylated DNA and immobilized on the slides. (E) The percentages of the folded conformation (E_{FRET} ~ 0.8) of Cy3Cy5-riboG-apt at 0–50.0 mM Mg^{2+} (cyan columns) and 0.5–100.0 mM Gua^{+} (red columns). (F) The percentages of the folded conformation of Cy3Cy5-riboG-apt change with Gua^{+} at 0, 0.5, 1.0 and 2.0 mM Mg^{2+}. (G) FRET histograms of Cy3Cy5-riboG-apt at 100.0 mM KCl (black curve), NaCl (green curve), urea (red curve) and guanidine (blue curve). The experiments were repeated for three times.

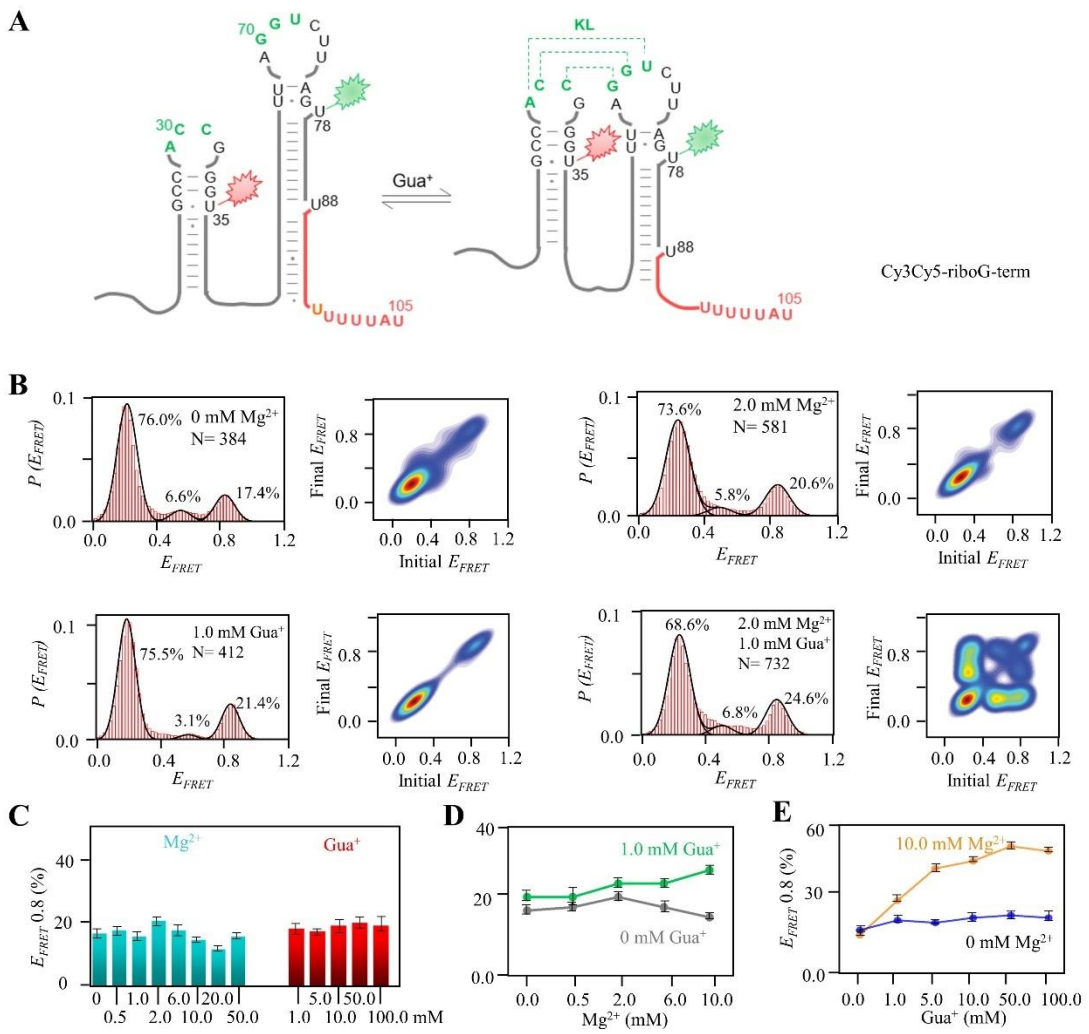

Figure 3. smFRET studies of post-transcriptional riboG-term at different concentrations of Mg^{2+} and Gua^{+}. (A) The secondary structures of Cy3Cy5-riboG-term at the unfolded (left) and the folded state (right). (B–E) smFRET histograms and transition density plots of Cy3Cy5-riboG-term at 0 mM Mg^{2+} (B), 2.0 mM Mg^{2+} (C), 1.0 mM Gua^{+} (D), and 2.0 mM Mg^{2+} and 1.0 mM Gua^{+} (E). (F) The percentages of the folded conformation (E_{FRET} ~ 0.8) of Cy3Cy5-riboG-term at 0–50.0 mM Mg^{2+} (cyan columns) and 1–100.0 mM Gua^{+} (red columns). (G) The percentages of the folded conformation of Cy3Cy5-riboG-term change with Gua^{+} at 0 (blue) and 10.0 mM Mg^{2+} (orange). (H) The percentages of the folded conformation of Cy3Cy5-riboG-term change with Mg^{2+} at 0 (black) and 1.0 mM Gua^{+} (green).

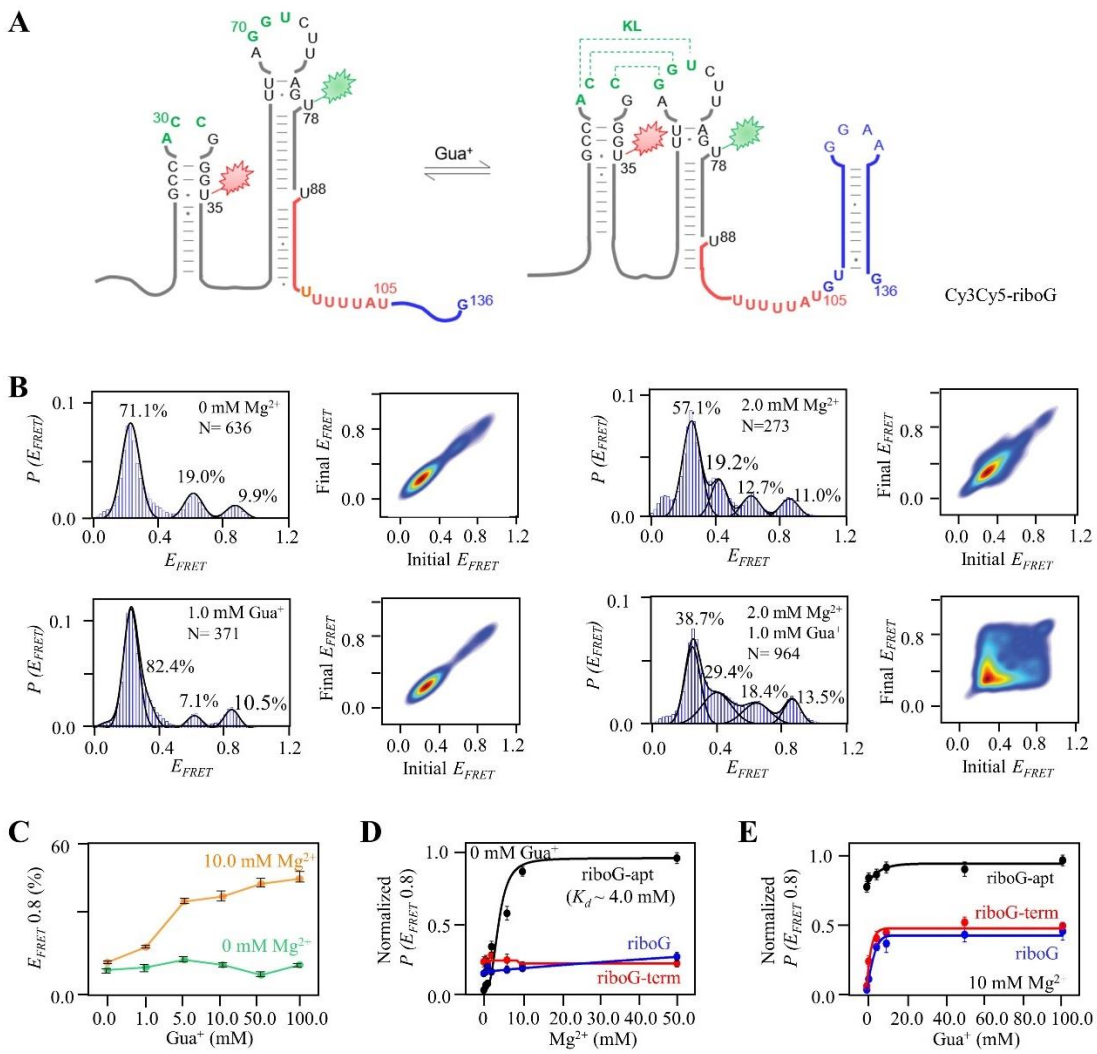

Figure 4. smFRET studies of the isolated riboG at different concentrations of Mg^{2+} and Gua^{+}. (A) The secondary structures of Cy3Cy5-riboG at the unfolded (left) and the folded state (right). (B–E) smFRET histograms and transition density plots for Cy3Cy5-riboG at 0 mM Mg^{2+} (b), 2.0 mM Mg^{2+} (C), 1.0 mM Gua^{+} (D), and 2.0 mM Mg^{2+} and 1.0 mM Gua^{+} (E). (F) The percentages of the folded conformation of Cy3Cy5-riboG change with Gua^{+} at 0 (green) and 10.0 mM Mg^{2+} (orange). (G–H) The normalized percentages of the folded conformation of Cy3Cy5-riboG-apt (black), Cy3Cy5-riboG-term (red) and Cy3Cy5-riboG (blue) at 0–50 mM Mg^{2+} (G) and 0–100.0 mM Gua^{+} in the presence of 10.0 mM Mg^{2+} (H).

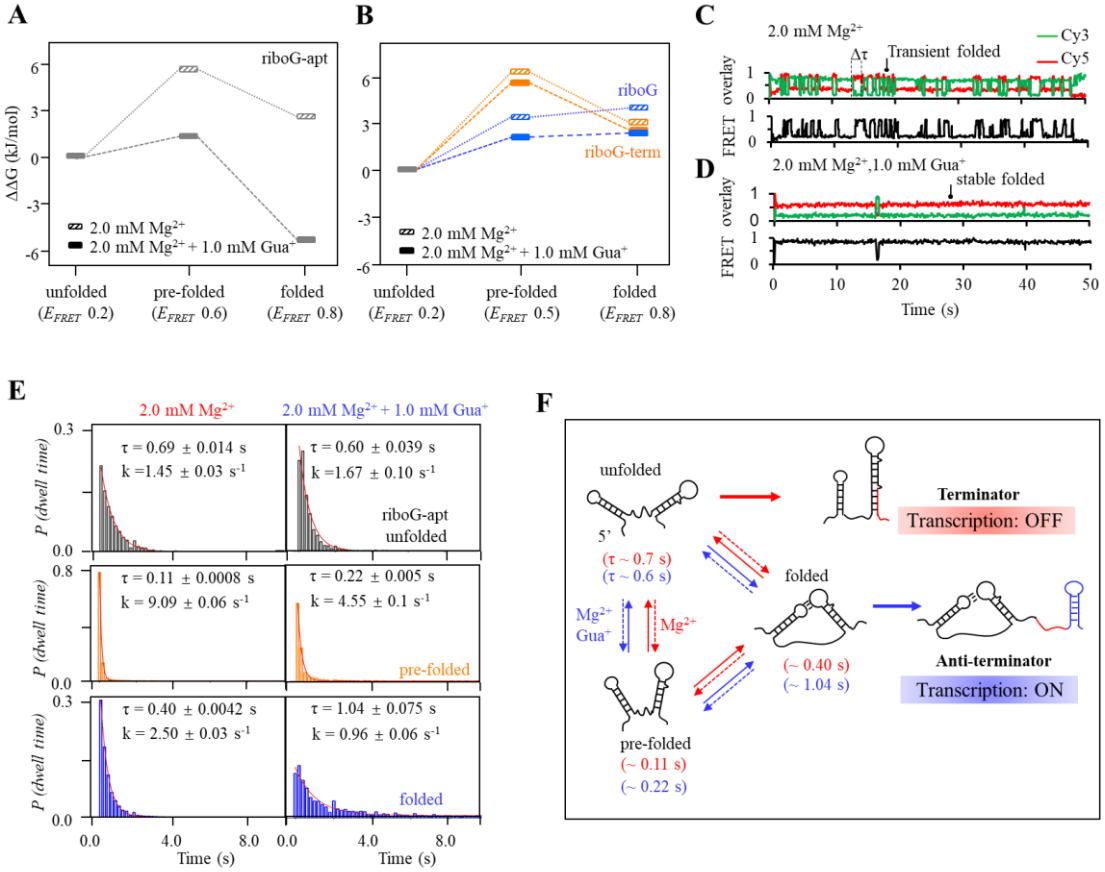

Figure 5. Relative free energy (*ΔΔG*) and kinetics analysis of isolated riboG-apt, riboG-term and riboG. (A) The relative free energy of the pre-folded and folded states of riboG-apt in the presence of 0 and 1.0 mM Gua^+ at 2.0 mM Mg^{2+}. The free energy of the unfolded state was referred as control. (B) The relative free energy of the pre-folded and folded states of riboG-term (orange) and riboG (blue) in the presence of 0 and 1.0 mM Gua^+ at 2.0 mM Mg^{2+}. (C–D) Representative time traces at 0 (C) and 1.0 mM Gua^+ (D) in the presence of 2.0 mM Mg^{2+}. Δτ is the dwell time. (E) The lifetime (τ) and rate constant (k) of unfolded (black), pre-folded (orange) and folded (blue) states of riboG-apt was determined by exponential decays of the dwell time distributions. (F) Schematic diagram of riboG-apt folding and transcriptional processes at 2.0 mM Mg^{2+} in the presence of 0 mM Gua^+ (red) and 1.0 mM Gua^+ (blue).

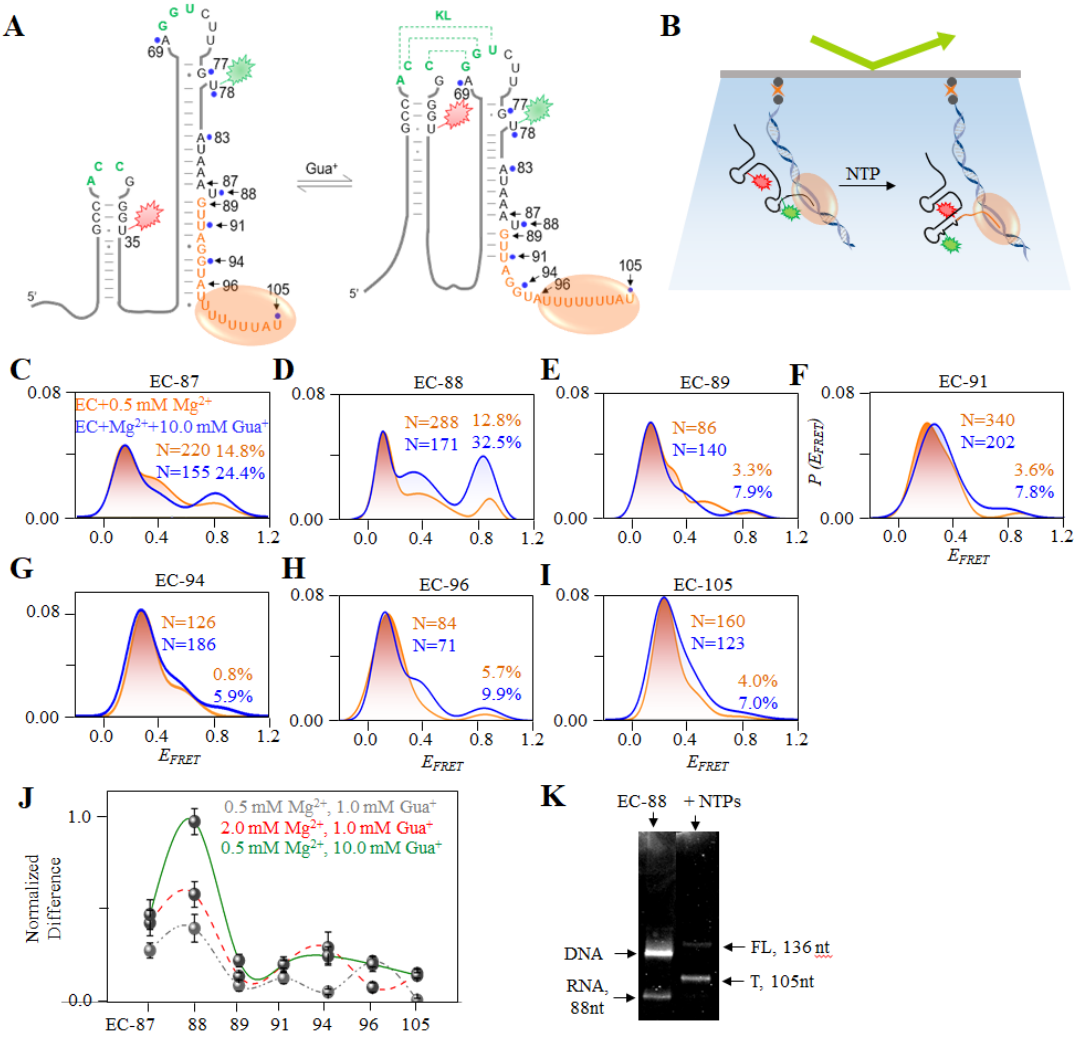

Figure 6. smFRET studies of nascent riboG in ECs without and with Gua$^+$ at 0.5 mM Mg^{2+}. (A) The ECs containing an RNA at the unfolded state (left) and the folded state (right). The pause sites of EC-87 to EC-105 are marked by black arrows, and the orange ellipse represents the RNA polymerase. (B) Schematic diagram for smFRET experiment for ECs. The ECs are immobilized on the slides by their biotinylated DNA templates. (C–I) smFRET histograms for the EC-87 to EC-105 at 0 mM (orange) and 10.0 mM Gua$^+$ (blue) at 0.5 mM Mg^{2+}. (J) The normalized increase of the folded conformation (E_{FRET} ~ 0.8) of ECs upon the addition of 1.0 mM Gua$^+$ at 0.5 mM Mg^{2+} (grey), 10.0 mM Gua$^+$ at 0.5 mM Mg^{2+} (green) and 1.0 mM Gua$^+$ at 2.0 mM Mg^{2+} (red). (K) The denaturing PAGE image of EC-88 elongation assay after overnight at room temperature.

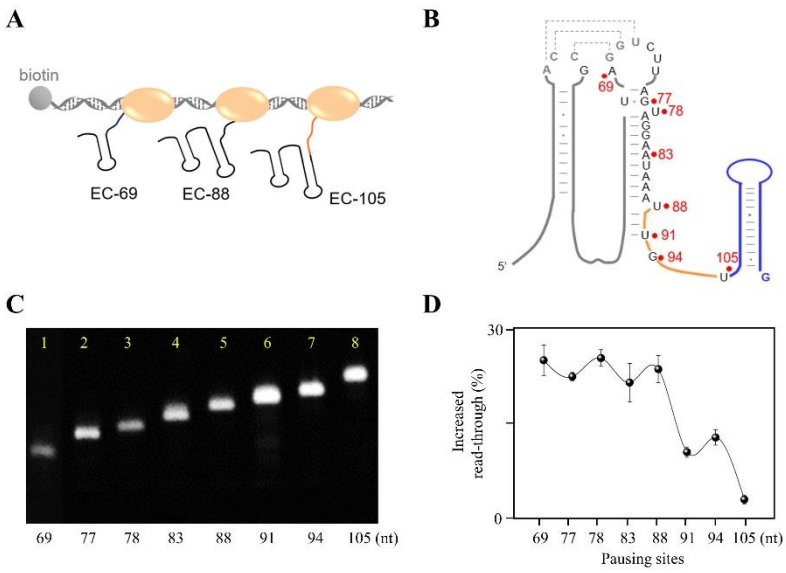

Figure 7. In vitro transcriptional performance of riboG. (A) The schematic diagram of synthesizing ECs with nascent RNAs by in vitro transcriptional pause using PLOR reactions. The orange ellipse represents RNA polymerase. (B) The secondary structures of riboG. The pause sites of EC-69, EC-77, EC-78, EC-83, EC-88, EC-91, EC-94 and EC-105 are marked by red dots. (C) The denaturing PAGE image of EC-69 to EC-105. The slow migration from EC-69 to EC-105 matches the growing lengths of RNAs. (D) The increase of transcriptional read-through upon the addition of 1 mM Gua+ with the last pause site at 69, 77, 78, 83, 88, 91, 94 and 105, respectively before completing transcription.

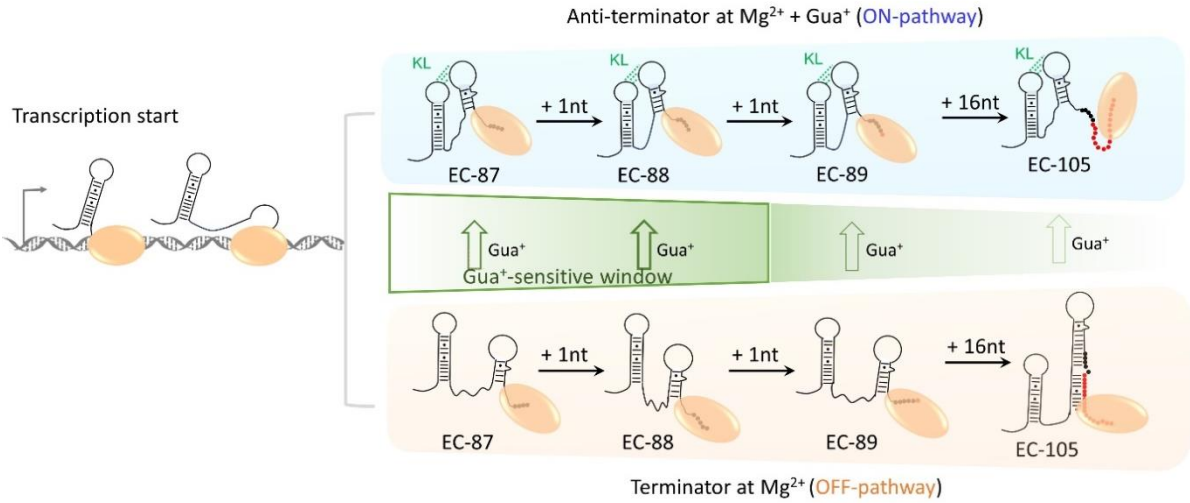

Figure 8. Folding model of RiboG in the absence and presence of guanidine. The folding pathways of anti-terminator conformation in the presence of Gua^+ and terminator conformation in the absence of Gua^+ are highlighted in blue and orange, respectively. The H-bonds in the KL are shown as dotted green lines. The nucleotides from EC-87 to EC-88 are shown as black dots, and the nucleotides in termination sequence are shown as red dots in EC-89 and EC-105. The RNAP is shown as orange ellipse. The DNA templates are shown as gray ribbons. Green arrows represent the direction of structural switching in native riboG upon the addition of the Gua^+. The thicker the arrow, the higher the switching percentages. And the Gua^+-sensitive transcription window of riboG from EC-87 to EC-88 is boxed by green lines.

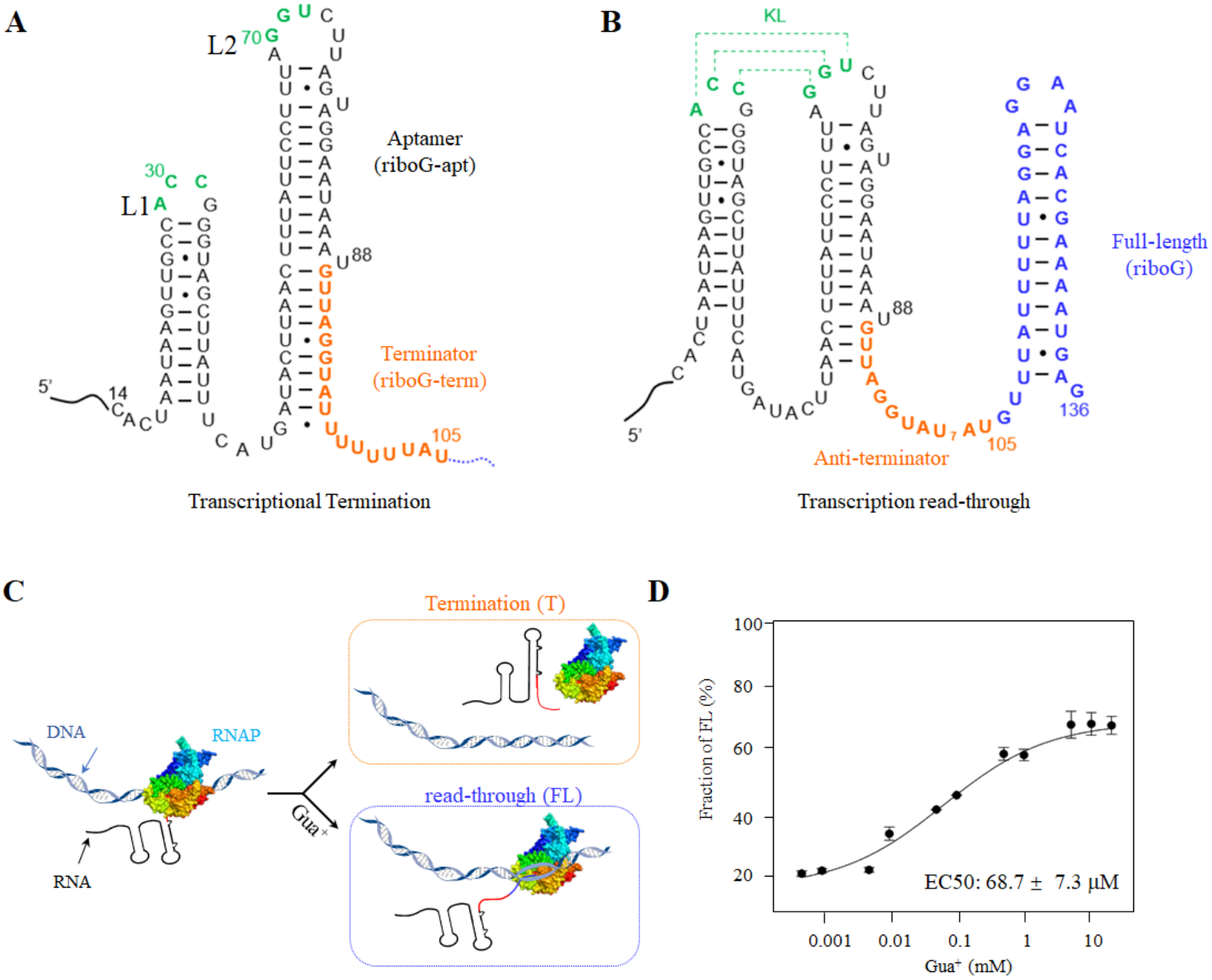
A
L2
L1
Aptamer
(riboG-apt)
Terminator
(riboG-term)
5'
Transcriptional Termination
B
KL
Full-length
(riboG)
Anti-terminator
5'
Transcription read-through
C
DNA
RNAP
RNA
Gua+
Termination (T)
read-through (FL)
D
Fraction of FL (%)
EC50: 68.7 ± 7.3 μM
Gua+ (mM)

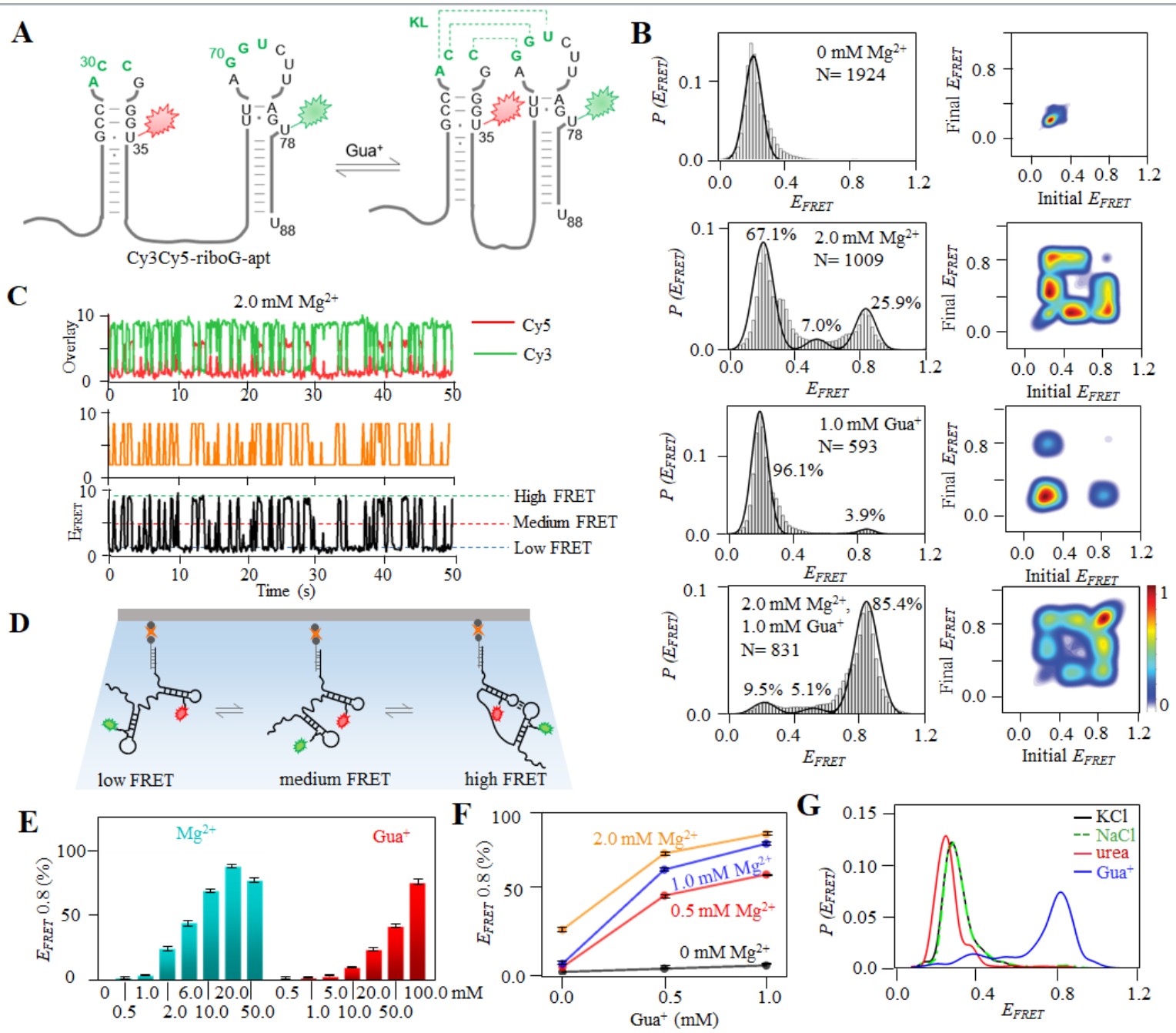
A
KL
Gua+
Cy3Cy5-riboG-apt
B
0 mM Mg2+
N= 1924
2.0 mM Mg2+
N= 1009
67.1%
25.9%
7.0%
1.0 mM Gua+
N= 593
96.1%
3.9%
2.0 mM Mg2+,
1.0 mM Gua+
N= 831
85.4%
9.5%
5.1%
P (EFRET)
EFRET
Final EFRET
Initial EFRET
C
2.0 mM Mg2+
Overlay
Cy5
Cy3
High FRET
Medium FRET
Low FRET
Time (s)
D
low FRET
medium FRET
high FRET
E
Mg2+
Gua+
EFRET 0.8 (%)
0 1.0 6.0 20.0 0.5 5.0 20.0 100.0 mM
0.5 2.0 10.0 50.0 1.0 10.0 50.0
F
2.0 mM Mg2+
1.0 mM Mg2+
0.5 mM Mg2+
0 mM Mg2+
EFRET 0.8 (%)
Gua+ (mM)
G
KCl
NaCl
urea
Gua+
P (EFRET)
EFRET

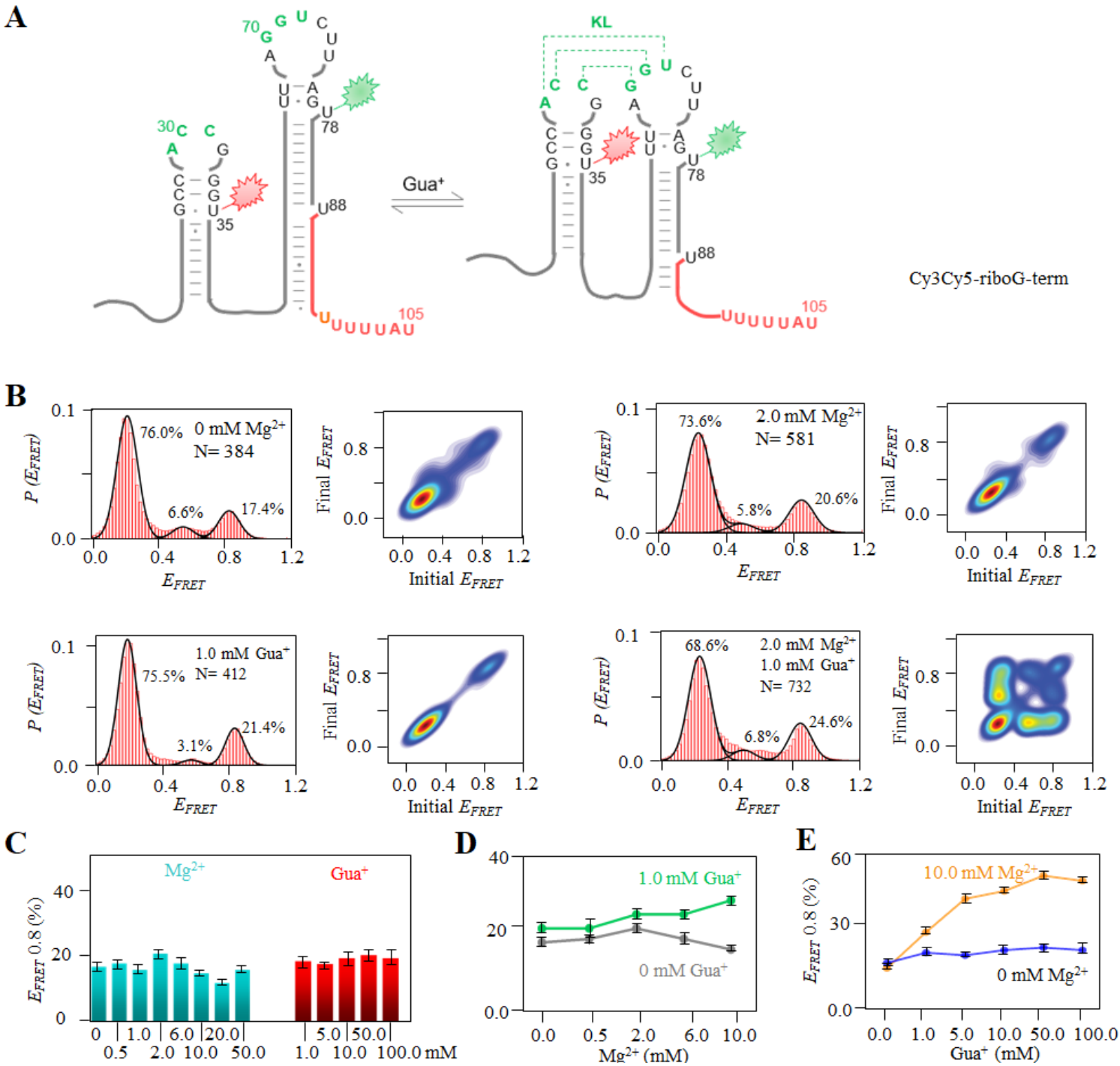
A
Gua+
KL
Cy3Cy5-riboG-term
B
0 mM Mg2+
N= 384
76.0%
6.6%
17.4%
2.0 mM Mg2+
N= 581
73.6%
5.8%
20.6%
1.0 mM Gua+
N= 412
75.5%
3.1%
21.4%
2.0 mM Mg2+
1.0 mM Gua+
N= 732
68.6%
6.8%
24.6%
P (EFRET)
EFRET
Final EFRET
Initial EFRET
C
Mg2+
Gua+
EFRET 0.8 (%)
0 1.0 6.0 20.0
0.5 2.0 10.0 50.0
5.0 50.0
1.0 10.0 100.0 mM
D
1.0 mM Gua+
0 mM Gua+
Mg2+ (mM)
E
10.0 mM Mg2+
0 mM Mg2+
Gua+ (mM)

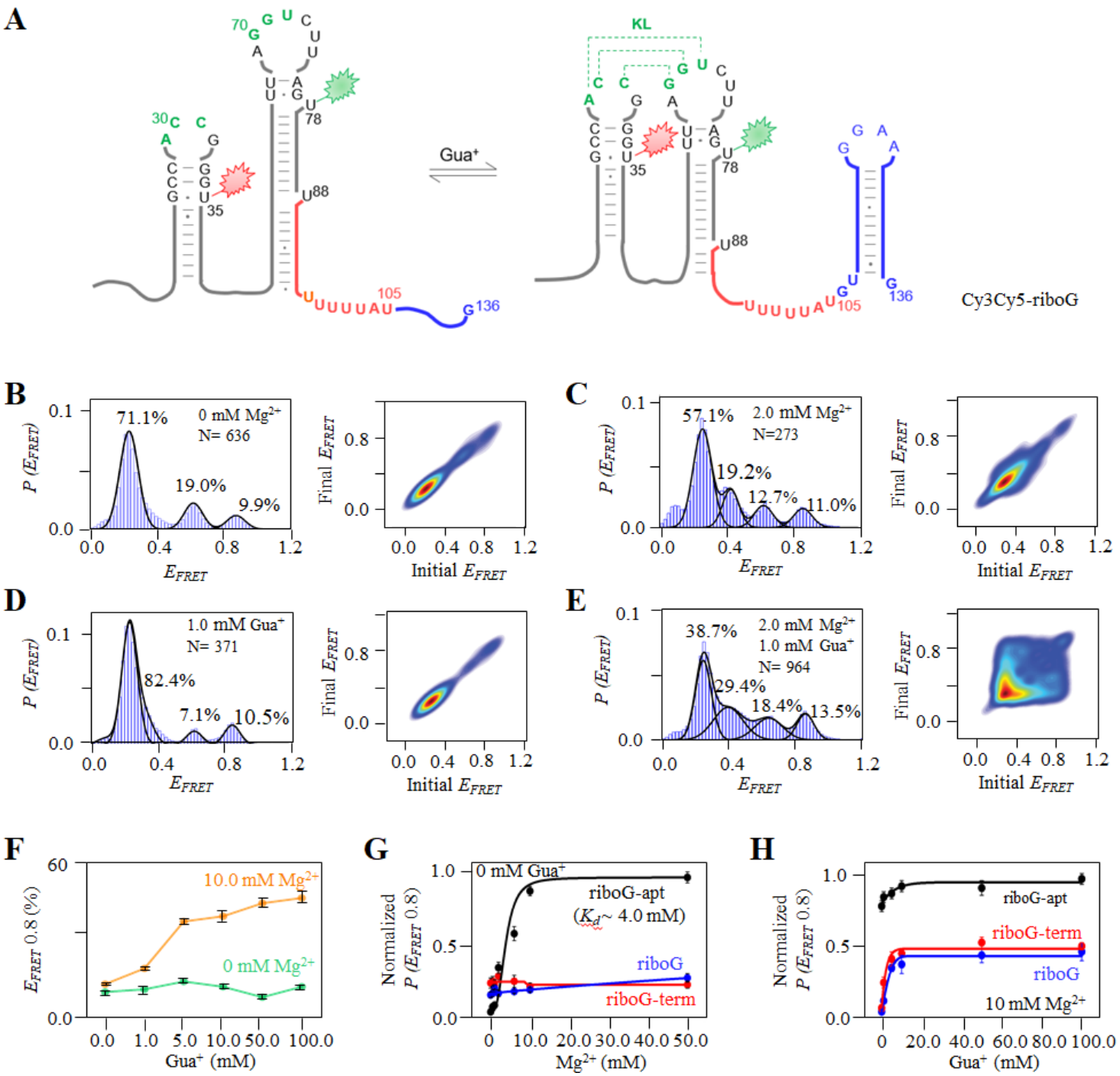
A
Gua+
KL
Cy3Cy5-riboG
B
71.1%
0 mM Mg2+
N= 636
19.0%
9.9%
P (EFRET)
EFRET
Final EFRET
Initial EFRET
C
57.1%
2.0 mM Mg2+
N=273
19.2%
12.7%
11.0%
D
1.0 mM Gua+
N= 371
82.4%
7.1%
10.5%
E
38.7%
2.0 mM Mg2+
1.0 mM Gua+
N= 964
29.4%
18.4%
13.5%
F
10.0 mM Mg2+
0 mM Mg2+
EFRET 0.8 (%)
Gua+ (mM)
G
0 mM Gua+
riboG-apt
(Kd~ 4.0 mM)
riboG
riboG-term
Normalized P (EFRET 0.8)
Mg2+ (mM)
H
riboG-apt
riboG-term
riboG
10 mM Mg2+
Gua+ (mM)

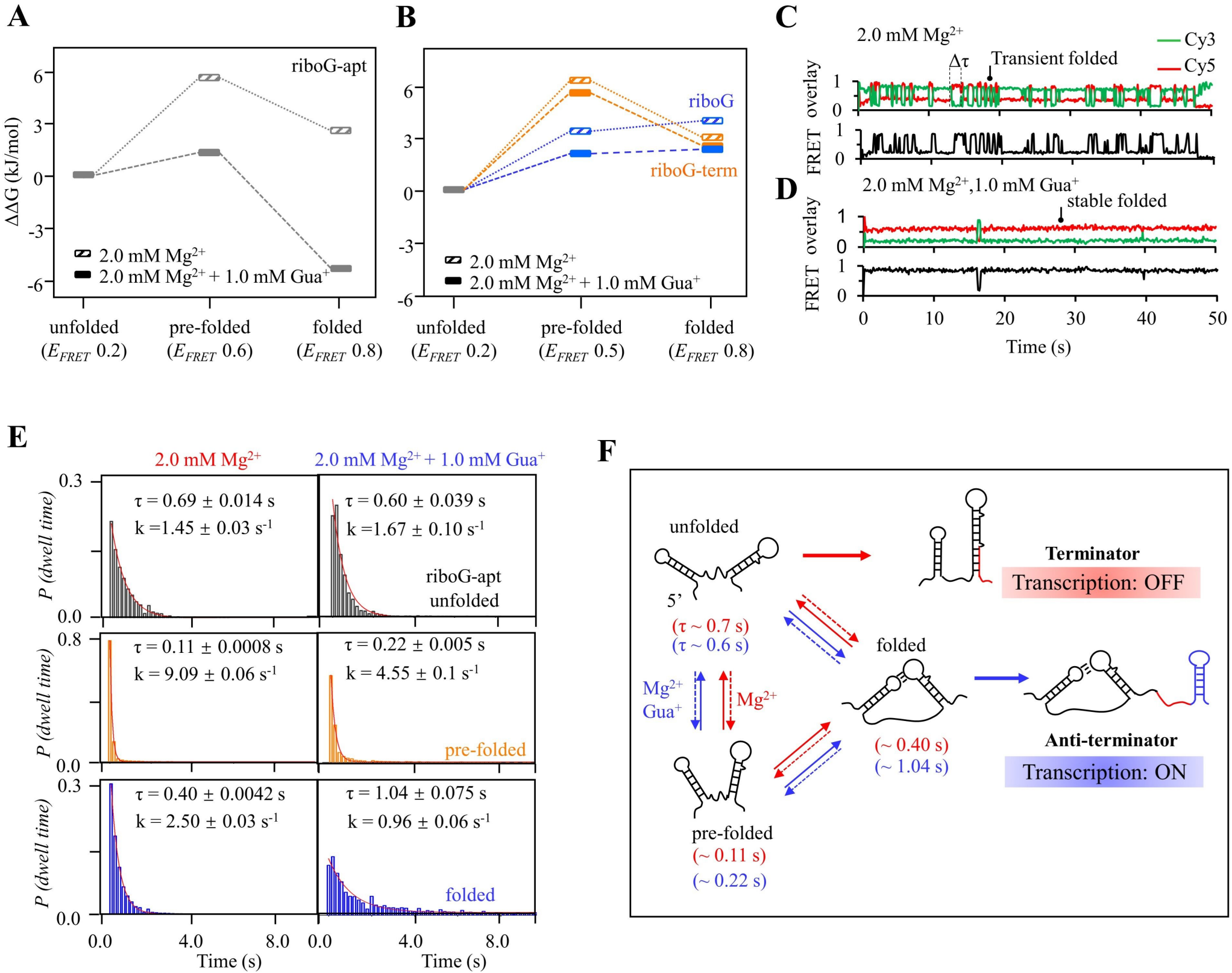
A
riboG-apt
ΔΔG (kJ/mol)
2.0 mM Mg2+
2.0 mM Mg2+ + 1.0 mM Gua+
unfolded (EFRET 0.2)
pre-folded (EFRET 0.6)
folded (EFRET 0.8)
B
riboG
riboG-term
2.0 mM Mg2+
2.0 mM Mg2+ + 1.0 mM Gua+
unfolded (EFRET 0.2)
pre-folded (EFRET 0.5)
folded (EFRET 0.8)
C
2.0 mM Mg2+
Δτ
Transient folded
Cy3
Cy5
overlay
FRET
D
2.0 mM Mg2+,1.0 mM Gua+
stable folded
overlay
FRET
Time (s)
E
2.0 mM Mg2+
2.0 mM Mg2+ + 1.0 mM Gua+
P (dwell time)
τ = 0.69 ± 0.014 s
k =1.45 ± 0.03 s-1
τ = 0.60 ± 0.039 s
k =1.67 ± 0.10 s-1
riboG-apt unfolded
τ = 0.11 ± 0.0008 s
k = 9.09 ± 0.06 s-1
τ = 0.22 ± 0.005 s
k = 4.55 ± 0.1 s-1
pre-folded
τ = 0.40 ± 0.0042 s
k = 2.50 ± 0.03 s-1
τ = 1.04 ± 0.075 s
k = 0.96 ± 0.06 s-1
folded
Time (s)
F
unfolded
5'
(τ ~ 0.7 s)
(τ ~ 0.6 s)
Terminator
Transcription: OFF
folded
Mg2+
Gua+
Mg2+
(~ 0.40 s)
(~ 1.04 s)
Anti-terminator
Transcription: ON
pre-folded
(~ 0.11 s)
(~ 0.22 s)

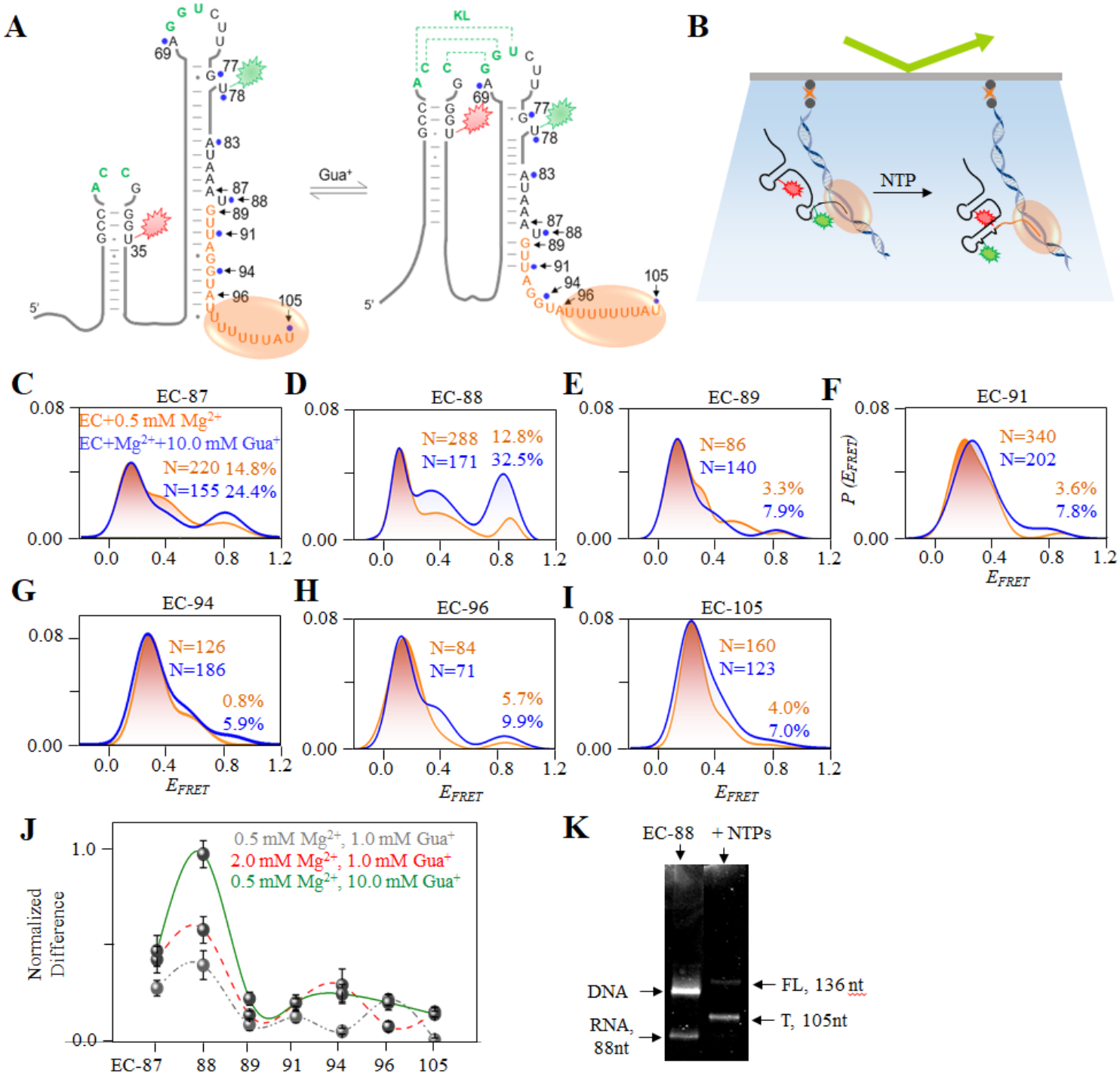
A
B
Gua+
KL
NTP
C
EC-87
EC+0.5 mM Mg2+
EC+Mg2++10.0 mM Gua+
N=220 14.8%
N=155 24.4%
D
EC-88
N=288 12.8%
N=171 32.5%
E
EC-89
N=86
N=140
3.3%
7.9%
F
EC-91
N=340
N=202
3.6%
7.8%
P (EFRET)
EFRET
G
EC-94
N=126
N=186
0.8%
5.9%
H
EC-96
N=84
N=71
5.7%
9.9%
I
EC-105
N=160
N=123
4.0%
7.0%
J
0.5 mM Mg2+, 1.0 mM Gua+
2.0 mM Mg2+, 1.0 mM Gua+
0.5 mM Mg2+, 10.0 mM Gua+
Normalized Difference
K
EC-88
+ NTPs
DNA
RNA, 88nt
FL, 136 nt
T, 105nt

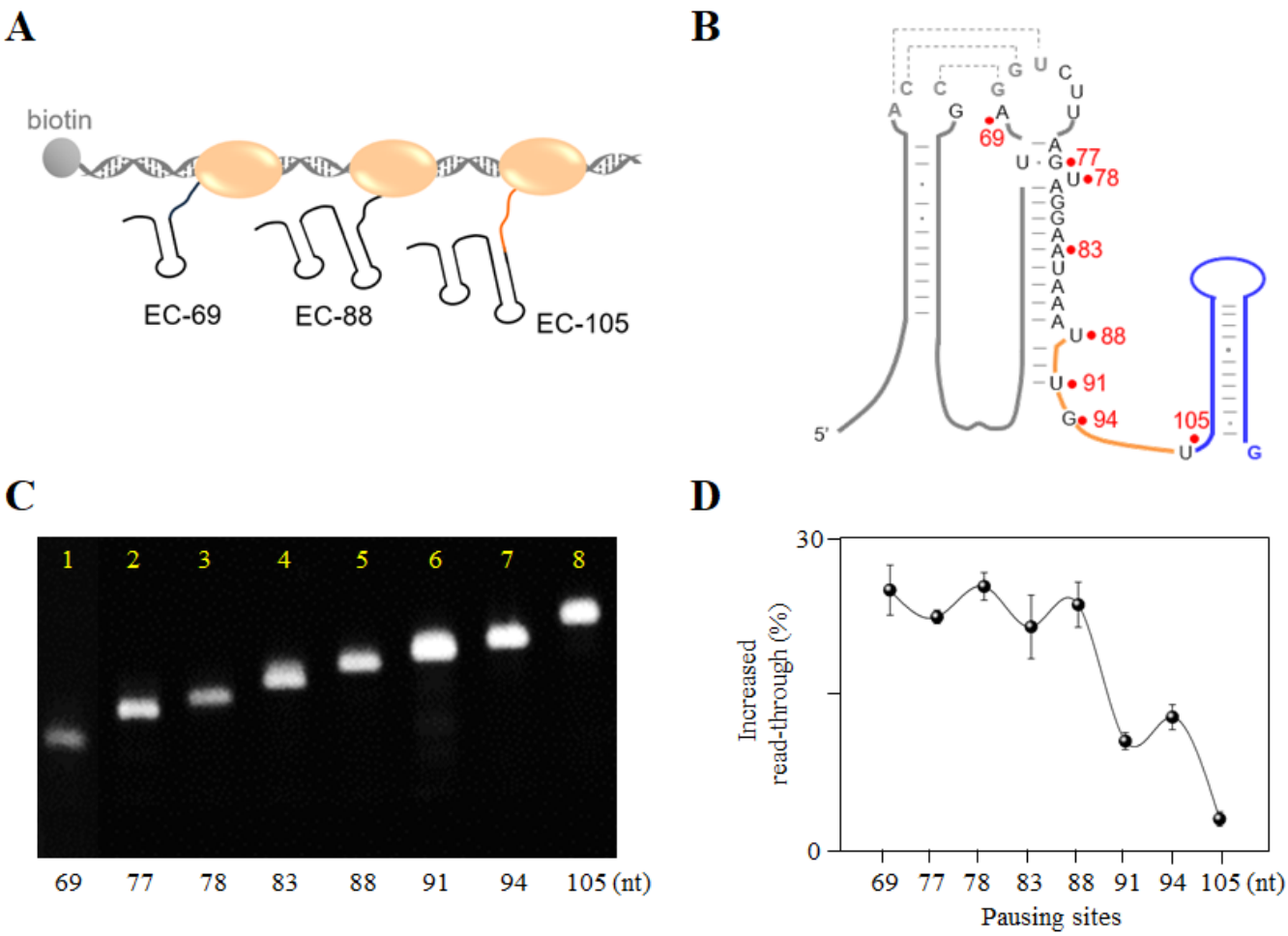
A
biotin
EC-69
EC-88
EC-105
B
69
77
78
83
88
91
94
105
5'
C
1
2
3
4
5
6
7
8
69
77
78
83
88
91
94
105 (nt)
D
30
0
Increased read-through (%)
69
77
78
83
88
91
94
105 (nt)
Pausing sites

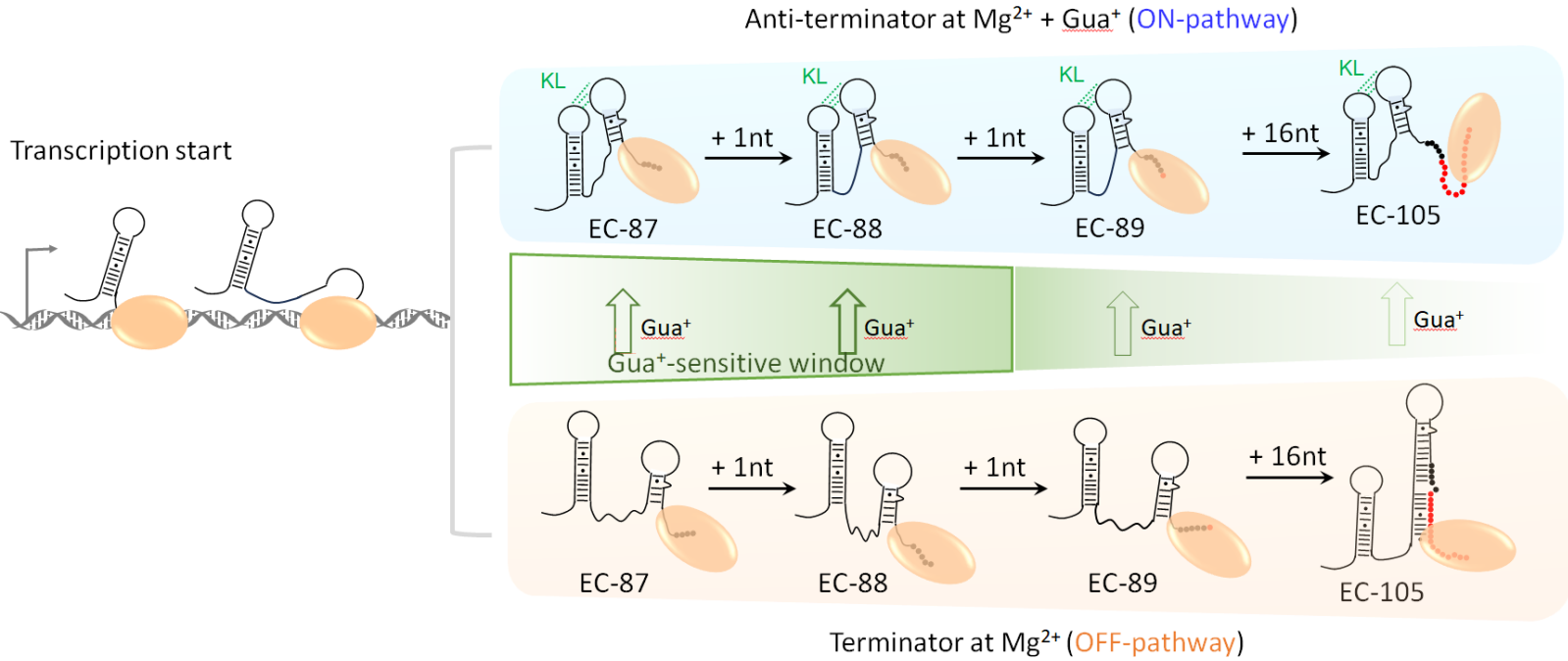
Anti-terminator at Mg2+ + Gua+ (ON-pathway)
Transcription start
KL
+ 1nt
+ 1nt
+ 16nt
EC-87
EC-88
EC-89
EC-105
Gua+
Gua+-sensitive window
Terminator at Mg2+ (OFF-pathway)